GEOMORPHIC AND SEDIMENTARY IMPACT ON BEACHES OF EASTERN VISAYAS (PHILIPPINES) AFTER TYPHOON HAIYAN IN 2013 – SHORT-TERM RECOVERY AND POST-DEPOSITIONAL CHANGES

Eva Quix, Max Engel, Fabian Boesl, Lia A. L. Gonzalo, Francesca V. Llanes, Mark A. C. Bahala, Rodrigo C. Eco, Jan A. M. Galang, Dominik Brill, S. Matthias May and Helmut Brückner

With 15 figures, 1 table and supplement
Received 26 March 2025 · Accepted 4 August 2025

Summary: Tropical cyclones and storm surges are a major threat to coastal communities of the Philippines. On 08th November 2013, category 5 Typhoon Haiyan (local name: Yolanda) made landfall on the islands of Eastern Visayas and caused more than 6000 casualties and severe damage to infrastructure and habitats. To assess the geomorphic impact of one of the strongest tropical cyclones on record, three post-typhoon surveys were conducted in 2014, 2015 and 2016 at two severely affected sites on the islands of Leyte and Samar. They aimed at documenting Haiyan-related erosional features and sand deposits. The sites have different geomorphic and geological settings, and exposure to the typhoon track. Differential global navigation satellite system (DGNSS) measurements and sediment analyses were used to document erosion and washover deposition caused by waves and coastal flooding of the beach ridge systems, as well as their recovery and changes over time. Shoreline changes were measured on high-resolution satellite images using the Digital Shoreline Analysis System (DSAS) to determine the typhoon's impact and recovery potential at a larger spatial scale. The results show the potential to identify storm-wave erosion and washover deposits in sandy ridge sequences across larger time scales. However, fine sedimentary signatures, such as millimetre-scale lamination, may be rapidly overprinted by bioturbation and geomorphic reorganisation of the coast. The coastline tends to return to its pre-storm equilibrium, whereas the pace depends on whether eroded sands remain within reach of the long-term wave regime, on the frequency of subsequent high-category storms and very local geomorphic conditions.

Keywords: Coastal erosion, erosional scarps, coastal hazards, tropical cyclone, Typhoon Yolanda, coastal geomorphology, palaeotempestology

1 Introduction

Low-lying coasts are constantly reshaped by tidal dynamics, sea-level change, land subsidence, long-term wave action, longshore currents, delta formation and extreme-wave events (storm surge and waves; tsunamis). When Typhoon Haiyan hit the Philippines on 08th November 2013, its strong winds, rain, waves and exceptional storm surge caused more than 6000 casualties and severe damage on infrastructure and habitats (Lagmay et al. 2015). The storm surge and wave setup had substantial geomorphic impact in Eastern Visayas (Region VIII), which is characterised by many beach-ridge systems (Brill et al. 2016, Soria et al. 2017, Switzer et al. 2020). These systems are usually formed by wave action above the mean high-water spring-tide level, where marine sands, pebbles or cobbles are deposited onshore and form the characteristic shore parallel, swash-aligned and often vegetated structures that are separated by low-lying swales (Hesp et al. 2005).

In contrast to their coarse-grained counterparts, sand ridges are rather built during moderate wave conditions and experience net erosion during extreme-wave events (Liew et al. 2010, Scheffers et al. 2012, Tamura 2012, Engel et al. 2015). Typical signatures of storm waves include erosional scarps at the youngest foredune (Tamura 2012, Dougherty 2014, Engel et al. 2015), breaches (Wang & Briggs 2015, Baumann et al. 2017), and laminated sand sheets or washover fans in the swales behind the first ridge (Kochel & Dolan 1986, Sedgwick & Davis 2003, Brill et al. 2016). These geomorphic and sedimentary features not only provide information on surge height and strength of current flooding events, but can also be used to decipher past events by means of age dating (May et al. 2013, Brill et al. 2015, Monecke 2020), sedimentological analysis (Engel et al. 2015, May et al. 2018) and geophysical imaging (Dougherty 2014, Dougherty et al. 2019, Baumann et al. 2017, Oliver et al. 2019, Monecke 2020).

https://doi.org/10.3112/erdkunde.2025.04.04 ISSN 2702-5985 (Online)

The potential of these methods to reconstruct processes of coastline evolution and extreme-wave events depends on site-specific factors and post-depositional modification, e.g., through rapid weathering and bioturbation. First, the extent and type of deposition and erosion patterns are influenced by the interaction of storm features (approaching angle, speed, storm surge, wave period and height) with coastal configuration, bathymetry and sediment availability (Schwartz 1982, Scheffers et al. 2012, Tamura 2012, Nott et al. 2015). After the event, the signatures are often overprinted by processes of geomorphic reorganisation, often within less than one year up to multiple years depending on the availability of sediment and the severity of the erosional event (Kümmerer et al. 2025), as well as by bioturbation and weathering. Especially in regions that are frequently (~1–10 years recurrence) hit by extreme waves, it is likely that specific sand layers and erosional signatures may not adequately represent the actual frequency pattern of prehistoric events (Otvos 2011, Scheffers et al. 2012, Tamura 2012). The geomorphic impacts of extreme storms, however, are dwarfed by those of major tsunamis, which can erode beach-ridge sequences for up to 500 m inland in a single event, potentially eliminating traces of previous events. The eroded sediments are often gradually transported back to the shore by regular wave action leading to almost complete coastal recovery within years (Liew et al. 2010, Monecke et al. 2015).

This potential of coastal recovery poses the question to what extent beach-ridge systems can serve as geo-archives for long-term event histories of extreme-wave events (Minamidate & Goto 2024, Leszczyńska et al. 2025). As the washover deposits and erosional imprints along the Eastern Visayan low-lying coasts were generated by a variety of partly site-specific processes such as storm surge, exceptionally high storm waves, tsunami-like surf beat (infragravity waves) and seiches during one of the strongest typhoons ever recorded, i.e. Typhoon Haiyan (Mori et al. 2014, Roeber & Bricker 2015, Soria et al. 2016, Tajima et al. 2016a,b), they may provide an important benchmark for this debate. The data on coastal recovery and shoreline changes may further be integrated into coastal protection measures and hazard management to better prepare coastal communities for future disasters and anticipate the potential impacts of these events.

In this paper, a combination of topographic survey, sedimentological analysis and multitemporal satellite imagery analysis is used to quantify the effects of storm surge and exceptional waves on beach-ridge systems of Eastern Visayas province in the Philippines. The data were collected during three post-typhoon field surveys in 2014, 2015 and 2016 at two study sites – Tolosa on Leyte Island, Dolores on Samar Island – that differ in terms of their geomorphic, geological, topographic and bathymetric setting as well as their exposure to Typhoon Haiyan's track (Fig. 1). The study aims at documenting (i) typhoon-induced erosional and depositional signatures in beach-ridge systems. In addition, we (ii) trace short-term coastal reorganisation and recovery processes, (iii) draw conclusions on the geomorphic resilience of coastal systems and (iv) discuss whether the post-depositional preservation of typhoon signatures is sufficient to use beach-ridge systems as a reliable archive for prehistoric events.

2 Study area

2.1 Geology and geomorphology

The Philippines archipelago was formed by collision and subduction processes between the Philippine Sea Plate and the southeastern edge of the Eurasian Plate. The boundary between these plates is defined as the Philippine Mobile Belt (PMB), a highly active tectonic convergence zone. It is composed of a more than 1200 km-long north-south running geological strike-slip fault system and two major subduction zones on both sides: the Manila Trench in the west and the Philippine Trench in the east (Aurelio & Pena 2002, Lagmay et al. 2009). Situated in this zone of intense deformation and seismic activity, the archipelago is composed of insular arcs, former continental crust, ophiolites and intermediate tectonic basins, forming coasts of alternating steep cliffs and alluvial, barrier-forming lowlands (Maeda et al. 2004, Bird 2010).

The island of Leyte is dominated by volcanoclastic and siliciclastic rocks and sediments, originating from its igneous core. The east coast, close to the study site of Tolosa, is characterised by low-lying alluvial beach-ridge plains, sandy beaches and sand spits formed by northward longshore drift (Suerte et al. 2005, Bird 2010). The offshore bathymetry in the funnel-shaped San Pedro Bay between Leyte and Samar declines rather gently to a maximum depth of 20 m, making the coast of Leyte prone to extreme storm surges (Soria et al. 2016, 2017) and amplifying seiches (Mori et al. 2014) (Fig. 1a).

The inner part of Samar, located northeast of Leyte, consists of Cretaceous to Oligocene ultrabasic to basic igneous rocks. In coastal areas they are often covered by a sequence of Pleistocene limestones

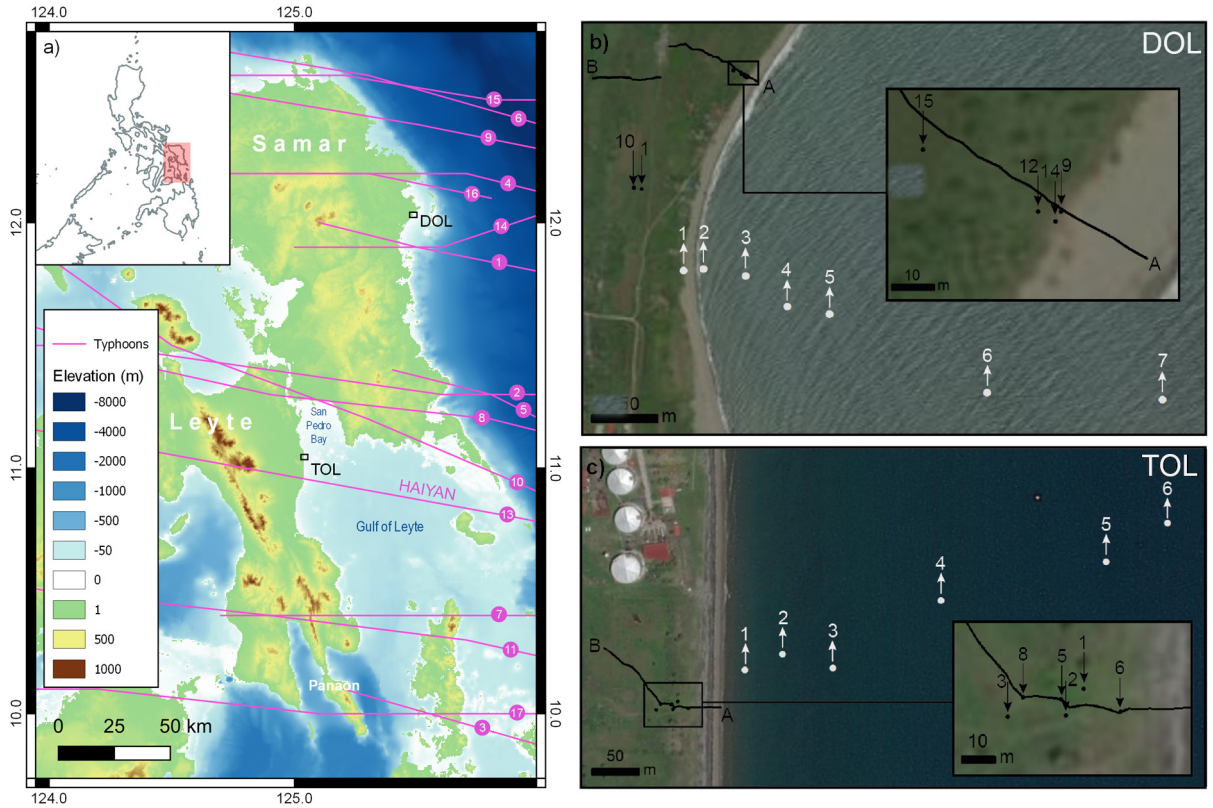

Fig. 1: Overview of the study area. (a) Philippine archipelago with location of the study sites in Eastern Visayas (islands of Leyte and Samar) and tracks of all typhoons since 1950 making landfall in the study area with SSHS intensity ≥3 as derived from IBTrACS (Knapp et al. 2010). White numbers refer to events listed in Table 1. Elevation and bathymetry are based on the GEBCO_2024 grid (GEBCO Compilation Group 2024). Location of sampling sites and topographical cross sections are illustrated for (b) Dolores (DOL) and (c) Tolosa (TOL) (based on ESRI base maps and SRTM data acquired from USGS). White dots indicate the location of offshore grab samples, black dots indicate sampling sites onshore.

and clastic sediments, forming terraces and cliff coasts with steep headlands and beaches in between (Traveglia et al. 1978, Ramos & Tsutsumi 2010). Around Dolores there are extended beach sections and sand spits supplied by longshore currents. Coral reefs are only present at the small island of Hilabaan, located approximately 7 km offshore, since the Dolores river provides high, clay-rich sediment loads (Traveglia et al. 1978) preventing coral growth between the island and the mainland. East of Hilabaan, the ocean floor steeply drops down to depths >8500 m towards the Philippine Trench (Fig. 1a).

2.2 General climate

The climate in the study area is maritime and tropical with a mean annual temperature of 26.6 °C and high humidity throughout the year. The annual rainfall (2659 mm for Tacloban, Leyte) is controlled by the summer monsoon and frequently crossing typhoons (PAGASA 2025a,b). On average, more than 20 tropical cyclones enter the Philippine Area of Responsibility (PAGASA 2025c) every year, 70% of which occur from July to October (PAGASA 2025d). Most typhoon systems originate in the Pacific Ocean and follow a northwesterly track, making the exposed east coasts of Luzon, Leyte and Samar particularly vulnerable to the hazards of wind damage, heavy rains, flash floods and coastal flooding (Lapidez et al. 2015). On the islands of Samar and Leyte (including Panaon Island), 17 typhoons made landfall since 1950 with intensities of ≥3 on the Saffir–Simpson hurricane scale (SSHS); eight of them reached category 4, two, including Haiyan, reached category 5 (Fig. 1a, Tab. 1).

2.3 Recent typhoons

Typhoon Haiyan, known as Yolanda in the Philippines, originated from a tropical depression over the northwestern Pacific on 03rd November

Tab. 1: Instrumentally recorded typhoons making landfall on either Samar or Leyte (including Panaon Island) with intensity of ≥3 on the Saffir-Simpson Hurricane Scale (SSHS). Data adapted from the IBTrACS database (Knapp et al. 2010) until June 2025. Wind = maximum sustained wind speed in knots (1-min mean).

No.	Name	Year	Month	SSHS	Wind (kt)	Landfall lat. (°N)	Island
1	Iris	1951	5	3	110	11.92	Samar
2	Wilma	1952	10	4	130	11.30	Samar
3	Emma	1952	7	3	100	10.09	Panaon
4	Gilda	1959	12	5	140	12.20	Samar
5	Irma	1966	5	3	100	11.34	Samar
6	Emma	1967	11	4	120	12.63	Samar
7	Nelson	1982	3	3	100	10.40	Leyte
8	Agnes	1984	11	4	120	11.22	Samar
9	Betty	1987	8	4	135	12.43	Samar
10	Skip	1988	11	4	120	10.99	Samar
11	Mike	1990	11	4	125	10.36	Leyte
12	Manny	1993	12	3	110	12.67	Samar
13	Haiyan	2013	11	5	168	10.96	Leyte
14	Hagupit	2014	12	3	105	11.90	Samar
15	Melor	2015	12	4	125	12.60	Samar
16	Vongfong	2020	5	3	98	12.16	Samar
17	Rai	2021	12	4	128	10.01	Panaon

2013, before intensifying and reaching typhoon status on 05th November. Haiyan reached greatest intensity with a maximum sustained wind speed of 315 km/h (SSHS category 5) shortly before landfall near Guiuan (Eastern Samar) on 08th November (Lagmay et al. 2015), close to the study sites of Dolores and Tolosa (Fig. 1a).

Between the first (February 2014) and the second (March 2015) survey, the coastline of Eastern Samar was hit by Typhoon Hagupit, another category 5 typhoon reaching a maximum sustained wind speed of 213 km/h. On 06th December 2014 it made landfall at Dolores, where it had weakened to 10-min maximum sustained winds of 167 km/h and SSHS category 3, still leaving substantial infrastructure damage behind (OCHA Philippines 2014, Tablazon et al. 2017). Two storms – local names Agaton (tropical depression on 19th January 2014) and Basyang (tropical storm on 01st February 2014) – passed close to Tolosa after Haiyan and before the first field survey but only reached maximum sustained winds of 100 km/h and 120 km/h, respectively (NDRRMC 2014a,b).

2.4 Storm surge and coastal flooding during Typhoon Haiyan

In Leyte Gulf, exceptional storm surge levels of up to 8 m and coastal flooding of >2 km inland were reported (Mas et al. 2015, Soria et al. 2016) due to south-north directed winds pushing the water into the shallow, funnel-shaped bay (Fig. 1a) and an additional contribution from seiches (Mori et al. 2014, Roeber & Bricker 2015, Takagi et al. 2017). The area of the study site at Tolosa experienced storm surge levels of ca. 5 m (Takagi et al. 2017) and maximum significant wave heights of 5–6 m (Watanabe et al. 2017). The peak inundation lasted for about two hours, with the most substantial damage within an area of approximately 200 m from the coast (Mas et al. 2015, Soria et al. 2016, 2017, Watanabe et al. 2017).

About 100 km further north of Haiyan's track, lower storm surge heights of ≤1 m were modelled for the area of Dolores (Lagmay et al. 2015, Takagi et al. 2017). Highest flooding levels in the area were recorded at Hilabaan (up to 4 m above mean sea level [msl], Quix 2018) mostly through maximum significant wave heights of >15 m along the open coast (Bricker et al. 2014, Tajima et al. 2016b). Typhoon Hagupit hit the not yet recovered coastline of the central to northern part of Eastern Samar with storm surge of ~3 m and high waves (Mühr et al. 2014).

3 Methods

Three post-typhoon surveys were carried out in February 2014 (only Tolosa, see Brill et al. 2016), March 2015 and July 2016 around Tolosa and Dolores (including the offshore island of Hilabaan).

The topography of all locations was documented along shore-perpendicular transects using a Topcon HiPer Pro differential global navigation satellite system (DGNSS) with a lateral and vertical error of <2 cm. All measurements were differentially corrected to the local tide level at the time of the survey based on tide predictions by WXTide software (Flater 1998). Samples of Haiyan's washover deposits were also taken at representative locations in these areas by means of push cores with lengths of 15–70 cm and hand-dug pits. During the second and third survey, similar sampling locations were chosen to study post-depositional changes of the typhoon signatures in the beach-ridge systems over the years. In 2016, additional offshore samples were taken with an Ekman-Birge grab-sampler between the intertidal and a distance of about 480 m from the shore in Tolosa and 1.5 km in Dolores in order to narrow down the source environment of onshore typhoon deposits.

3.1 Sedimentological and geochemical analysis

After high-resolution sampling of the onshore push cores at 1–2 cm intervals, the samples were dried and granulometric measurements were carried out using dynamic image analysis (Camsizer, Retsch GmbH) covering a particle-size range between 0.03 and 30 mm. Grain-size analysis of the finer-grained offshore samples (<2 mm) was conducted using a laser particle analyser (Beckmann Coulter LS 13320) after pre-treatment with H_2O_2 (15%) to remove organic matter and $Na_4P_2O_7$ (46.7 g/l) for aggregate dispersion. Univariate statistical measures after Folk & Ward (1957) were calculated using GRADISTAT software v8.0 (Blott & Pye 2001). Geochemical analyses of the deposits were conducted by determining the carbon (C) and nitrogen (N) composition of push core DOL 14 using an Elementar vario EL cube elemental analyser with a detection limit of <0.1 %. Ground sample material (~20 mg) was folded into tin containers and combusted at 950 °C.

3.2 Digital shoreline analysis

In order to determine the post-typhoon coastal recovery, shoreline locations on pre-Haiyan Pléiades satellite images with a resolution of 0.5 m were compared with post-Haiyan images captured directly after the typhoon (November 2013) and in May 2015 (Tab. S1). The satellite images were aligned by utilising stable control points such as houses and crossroads in ESRI ArcGIS software. The shoreline was extracted on all georeferenced and orthorectified images by reflectance values from red and near-infrared wavelengths using the image classification tool of ArcMap (Lipakis et al. 2008, García-Rubio et al. 2009). The tool separates satellite images into two clusters corresponding to water and land by using manually created training samples. The border between the two clusters roughly complies with the tonal contrast of the wet and dry part of the beach, indicating the approximate high-water line (HWL), which is generally considered the best shoreline indicator in multi-temporal satellite image analysis (Pajak & Leatherman 2002, Lipakis et al. 2008, Monecke et al. 2015). Manual editing of the calculated shorelines was applied in areas where obvious errors occurred, for example due to mangrove cover of areas belonging to the sea. Occasional gaps in shoreline coverage occur due to cloud cover.

Rate-of-change-statistics were computed using the Digital Shoreline Analysis System (DSAS) (Thieler et al. 2009). Several shore-perpendicular transects with a 50 m spacing were established to calculate the net shoreline movement (NSM), defined as the distance between two selected shorelines and directly reflecting coastal retreat or progradation (Fig. S1). Transects crossing areas of obvious anthropogenic alteration (i.e. villages, roads) were excluded prior to calculation. In total, more than 80% of the transects along the 12 km (Tolosa) and 16 km (Dolores) coastal stretches were included in the calculation.

3.3 Shoreline positioning errors

Shoreline positioning errors may occur due to the resolution of the images, georeferencing offsets, errors resulting from the previous shoreline extraction or unknown tidal ranges at acquisition time of the satellite images (cf. Monecke et al. 2015). The first two uncertainty terms are considered negligible because of the high resolution of the satellite images (Hapke et al. 2010, Ruggiero et al. 2013). Errors derived from shoreline extraction are minimised by the usage of training samples to differentiate land from water and can be excluded as well (Lipakis et al. 2008). To account for the natural migration of the HWL with seasonal changes and tidal variations, horizontal shoreline variations were calculated by using basic trigonometry (cf. Morton et al. 2004,

Monecke et al. 2015). Due to the microtidal regime both in Dolores (maximum range = 1.16 m, i.e. 0.27–1.43 m above the lowest astronomical tide [LAT]) and Tolosa (maximum range = 0.81 m, i.e. 0.10–0.91 m above LAT), vertical high tide differences of less than 0.3 m can be assumed. Considering an average beach slope tan β as derived from the DGNSS transects, this leads to horizontal shoreline changes of ±10 m (Dolores) and ±5 m (Tolosa). The highest potential errors, however, are associated with variable run-up (Monecke et al. 2015), which could not be calculated because of lacking information on wave height (Masselink et al. 2011). Instead, a value of 10 m was chosen tentatively as a maximum estimate that should include all potential run-up variations, especially considering the moderate tidal range at both investigated sites. From these two uncertainty terms, the total uncertainty value for every shoreline position was calculated as the square root of the sum of squares (Ruggiero et al. 2013), which results in a total shoreline position uncertainty of ±11.2 m for Tolosa and ±14.1 m for Dolores (Tab. S2).

4 Results

4.1 Erosional and depositional signatures of Typhoon Haiyan

At both sites, the beach ridges were completely inundated during the typhoon. Beaches and berms were eroded and sediment with grain sizes ranging from mud to sand was transported across the first ridge and accumulated on top of the ridge and in the back-barrier swale.

4.1.1 Tolosa (TOL), Leyte

At Tolosa, Leyte Island, the coastal barrier and the back-barrier depression were inundated with a maximum height of 4.7 m above msl, reaching landward inundation limits of up to >1000 m (Brill et al. 2016, Watanabe et al. 2017) (Fig. S2). Erosion left a distinct scarp, synchronously filled with sand, to some extent (Fig. 2a). By the time of the 2015 survey, the recovery of the beach had proceeded, and the

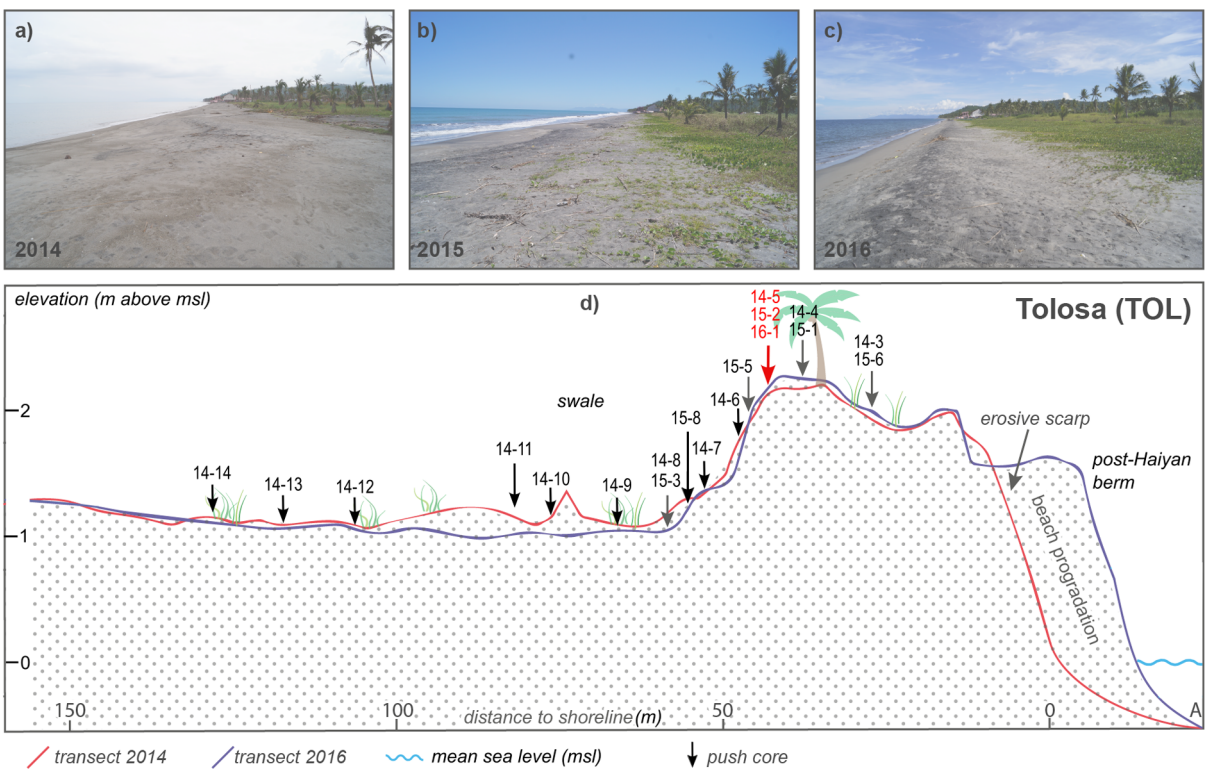

Fig. 2: Coast recovery in Tolosa. (a) After complete inundation and heavy beach erosion in 2014, (b) subsequent reworking of sand and the re-establishment of vegetation, mostly *Ipomoea pes-caprae* (beach morning glory), (c) led to the formation of a new beach ridge until 2016, (d) which is demonstrated by two shore-perpendicular transects. Note the accumulation of sand on top of the ridge whereas the ground has flattened in the back-barrier swale after two years (msl = mean sea level). The master profile is indicated by a red arrow and shown in Fig. 4.

scarp was overprinted by vegetation and the formation of a new berm, which had prograded further and became steeper by 2016 (Fig. 2b,c).

At Tolosa in 2014, the deposition of sandy material terminated c. 150 m from the shoreline as a sheet of grey sand with a maximum thickness of 10–20 cm on the leeward site of the barrier (50–60 m from the shore). The thickness rapidly declined to only a few millimetres >90 m from the shoreline (Fig. 3a), where it also became finer (Fig. 3b). The storm deposits on top of the beach ridge were clearly visible against the underlying dark brown soil and characterised by a laminated structure of alternating siliciclastic material (light) and greyish black heavy mineral concentrations. This lamination was restricted to the top and back of the barrier and represented the washover fan (Unit 2). Unit 1 slightly coarsened in the upper part, where the lamination changed from horizontal (Unit 2, Layer II) to cross-bedded (Unit 2, Layer III) (Fig. S3). Towards the back-barrier depression it was overlying the landward-thinning and fining massive sand sheet (Unit 1 in Fig. 2). In 2015, progressive mixing due to root penetration blurred the lamination of Unit 2 (Fig. 4). The pattern of grain-size distributions with a coarsening up in the lower part (Unit 2, Layer II) and an overall coarser upper part (Unit 2, Layer III) of the washover fan deposit was still visible (Fig. 5). However, in 2016 the lamination had completely vanished (Fig. 4). In the back-barrier depression, the >10 cm thick grey sand sheet was almost completely mixed with the underlying soil within less than two years (cf. TOL 15-8, Fig. S4). Topographic surveying also revealed a levelling of the surface in this area (Fig. 2d). In contrast, sediment was accumulated at the top and the seaward side of the barrier between 2014 and 2016, and the

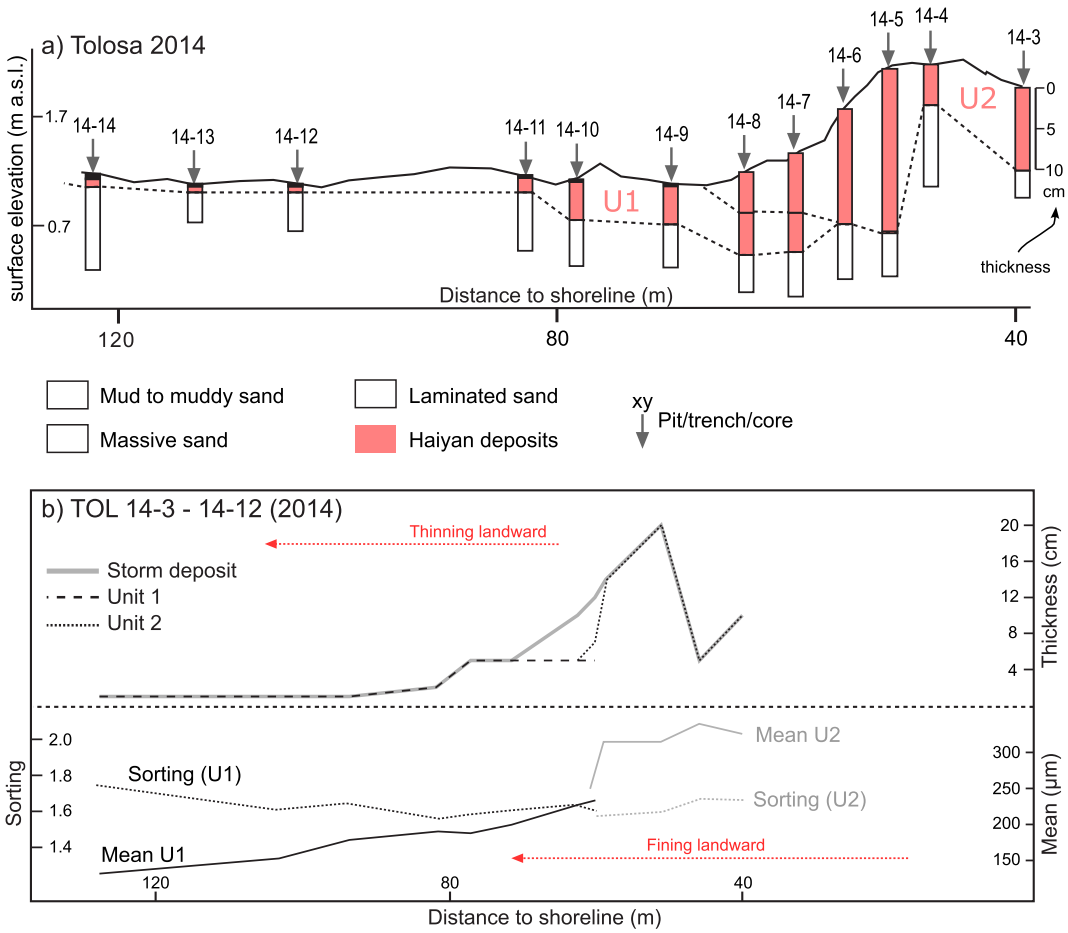

Fig. 3: The deposit of Typhoon Haiyan as documented and sampled three months after the typhoon (modified after Brill et al. 2016). a) Thickness and composition of typhoon deposits along the shore-perpendicular transect recorded in 2014 (for more details see high-resolution laboratory data for TOL 14-5 in Figure S3). The mostly massive basal Unit 1 (U1) is covered by the laminated Unit 2 (U2) in the proximal part of the coastal plain (TOL 14-3–14-8). b) Landward thinning and fining in typhoon deposits from Tolosa as documented for samples taken three months after Typhoon Haiyan.

Fig. 4: Temporal alteration of storm signatures in the washover deposit at Tolosa (location TOL 14-5, 15-2, 16-1). In 2014, the storm deposit was characterised by a sharp lower contact (note the pre-existing, now sand-filled cavity) and fine lamination of alternating siliciclastic material (light) and heavy minerals (dark) (Unit 2 in Fig. 3a, Fig. S3). In 2015, both the lower contact to the thin and capped light brown pre-Haiyan soil (40–50 cm below surface) and the lamination pattern became blurred; the older, very thick dark-mineral layers below the capped soil have lost their fine-lamination structure due to weathering and bioturbation. In 2016, the lamination of the Haiyan deposit was gone, the lower contact becomes gradual.

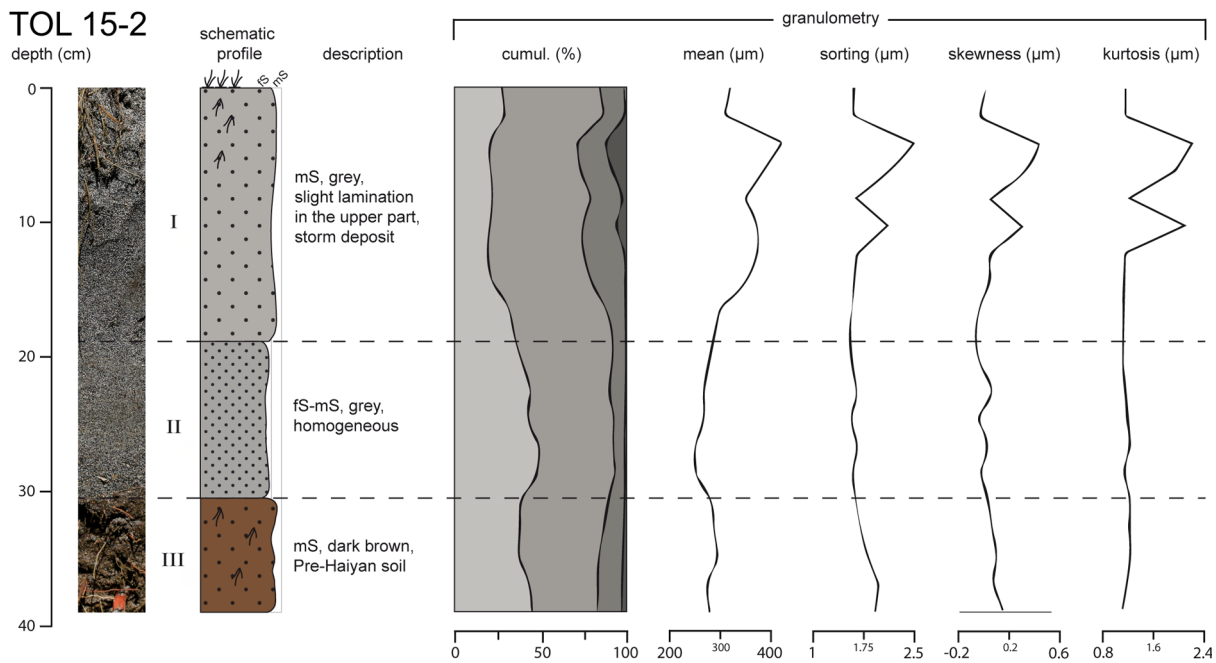

Fig. 5: Sedimentary characteristics of TOL 15-2. Within the Haiyan-related Unit 2 (layers II + III), Layer III is coarser than II and shows faint lamination, whereas the differences seem to be less distinct compared to 2014 (TOL 14-5 in Fig. S3). Both layers can still be clearly separated from the pre-Haiyan soil (Layer I).

respective push cores showed a post-Haiyan increase in thickness of the greyish deposit of up to 30 cm (cf. TOL 15-6, Fig. S5).

4.1.2 Dolores (DOL), Samar

In Eastern Samar, similar inundation limits of up to 800 m and onshore flow depths of 6–14 m were modelled (Shimozono et al. 2015) and reported (Brill et al. 2016, Soria et al. 2017) during Typhoon Haiyan. However, due to the time passed since Haiyan, no flood marks were found in trees or bushes of the prograded beach-ridge plain during the first survey at Dolores in 2015. In contrast to Tolosa, an erosive scarp of 1.7 m height (3.3 m above msl) was still preserved at the back of the active beach (Fig. 6a,d). Overwash of the barrier system was indicated by fresh sedimentation of sand, starting on top of the partly eroded ridge with a rapidly decreasing thickness inland. In 2015, the storm deposit had a maximum thickness of 18 cm in DOL 9, directly at the erosional scarp (Fig. S9). Even though there was no clear colour or sedimentary difference, a thin, brownish crust on top of the pre-Haiyan soil marked the boundary between the greyish brown, moderately sorted medium sand of the storm deposit and the previous surface. Below the deposit, layers of greyish brown medium sand alternated with light to dark brown sand with incipient soil formation (DOL 9, Fig. S9). Several pieces of plastic and glass bottles were embedded into the sand down to a depth of about 50 cm (Fig. 7b).

Locally, accumulation of sandy storm deposits must have reached at least 160 m inland, since a thin layer (2 cm) of the deposit covered the soil in DOL 1 (documented in 2015; Fig. 7, Fig. S10) which is located inside the first swale (Fig. 1b, 6d). Within the darker-coloured substrate, another layer of the same greyish brown material and varying thickness was located between 12 and 19 cm depth of the profile. The rest of the stratigraphic profile of DOL 1 resembled the structure at the erosive scarp with alternating layers of lighter and darker medium sand that slightly differed in organic content (Fig. 7, Fig. S10).

In 2016, the thickness of the storm deposit had decreased in all stratigraphic profiles on top of the beach ridge, reaching from 8 cm (18 cm in 2015) at the erosive scarp (DOL 14, Fig. 8) to 2 cm in DOL 12 c. 40 m from the shoreline (Fig. 9). In the swale be-

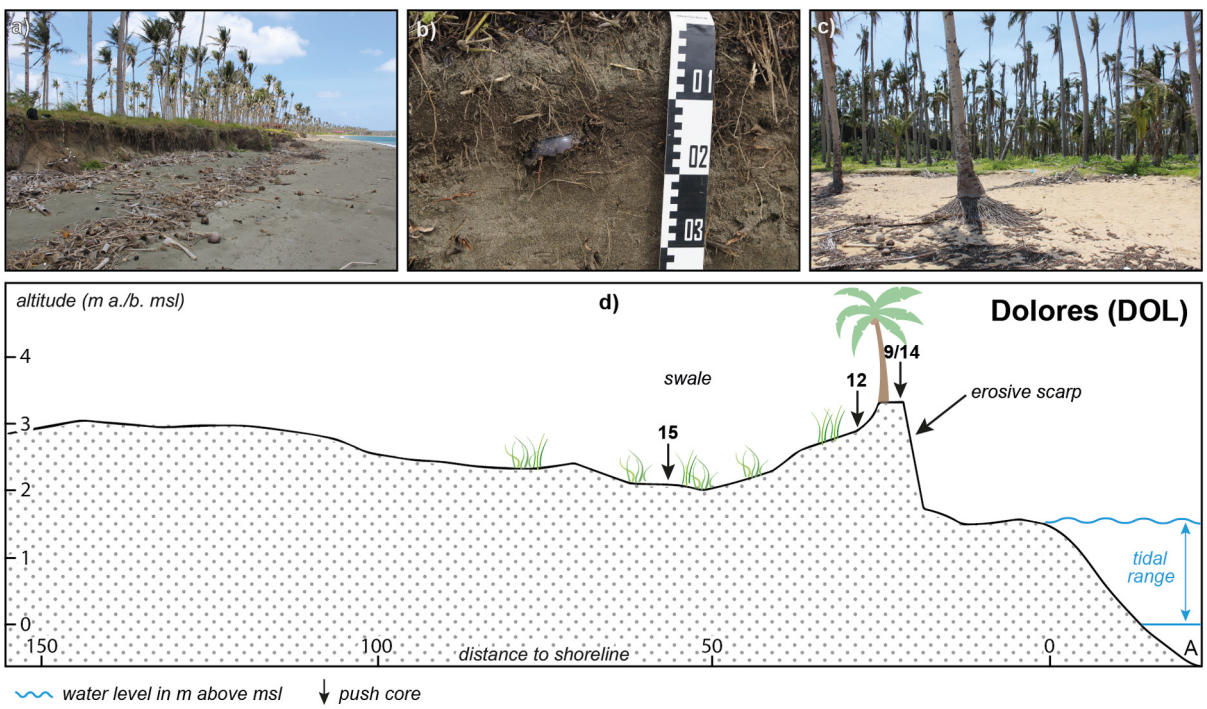

Fig. 6: Typhoon signatures at Dolores (Fig. 1b). (a) Accumulated drift wood at the bottom of the erosive scarp in 2015. In 2016, parts of the beach were already covered by vegetation. (b) Several glass and plastic pieces were embedded in the storm deposits. (c) Exposed palm roots on Hilabaan Island (~7 km off the coast) indicating erosion during Typhoon Haiyan. (d) Topographical cross section covering the northern sampling sites at Dolores illustrating the erosive impact of Haiyan on the beach-ridge system of Dolores (2015).

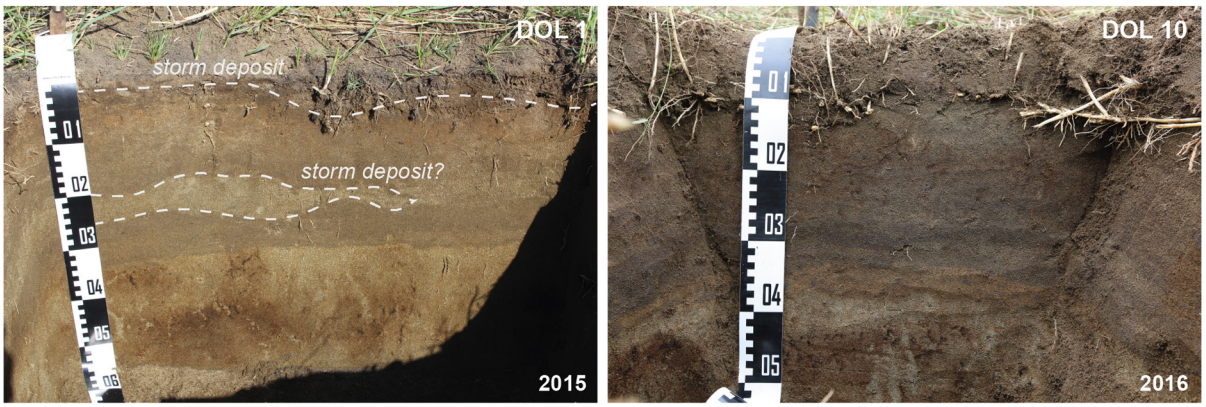

Fig. 7: Temporal alteration of storm signatures at Dolores (Fig. 1b). The stratigraphic profile of DOL 1 (2015) (cf. Fig. S10) was covered by a thin storm deposit (~2 cm). Another potential subrecent storm layer was situated between 20 to 25 cm depth (corresponds to 12–19 cm in Fig. S10) based on lighter colouring of the sand and very sharp boundaries. DOL 10 (2016) shows the site of DOL 1 in 2016, with the storm deposits mixed and incorporated into the surrounding soil by bioturbation.

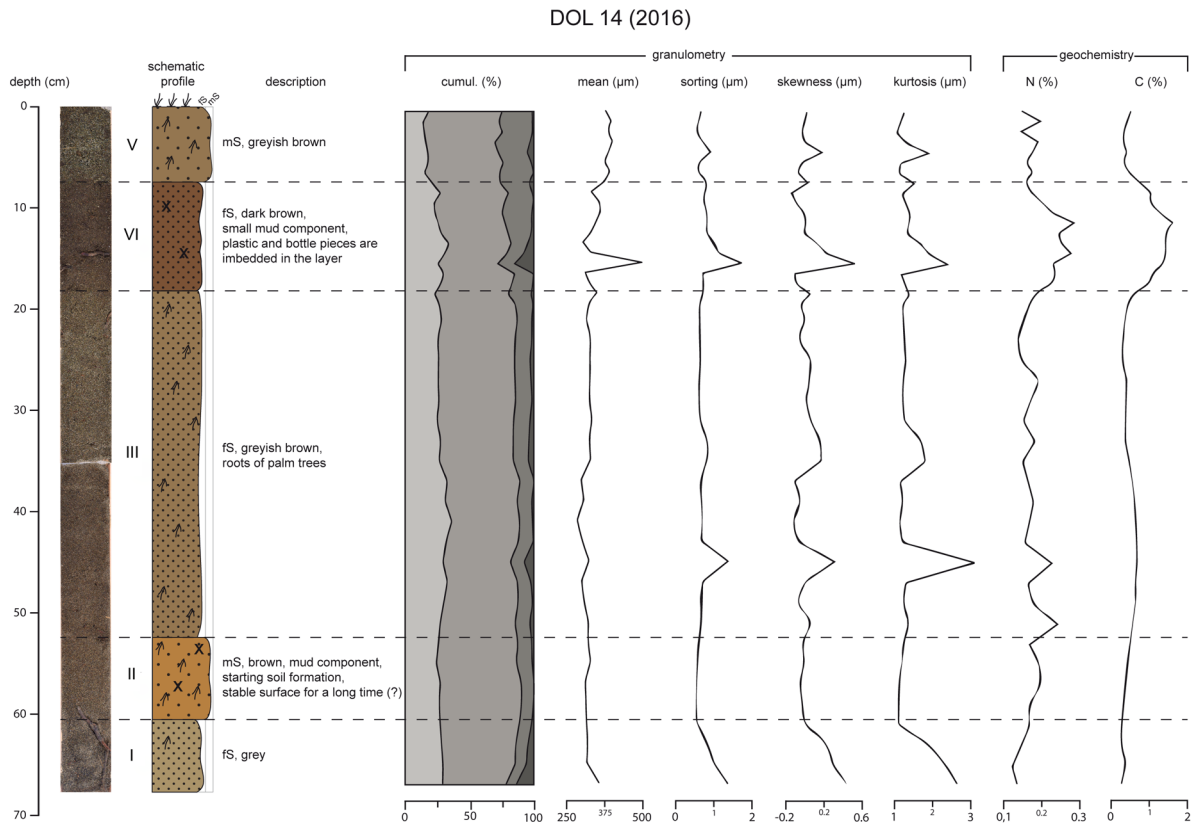

Fig. 8: Sedimentary and geochemical characteristics of DOL 14 (2016) at the erosional scarp. Layer V represents the Haiyan deposit, IV is the pre-Haiyan incipient soil formed in the barrier sand (Layer III). For a legend see Fig. 5.

hind the ridge, traces of the storm deposit, identified in 2015, were no longer visible (Fig. S11, Fig. S12). Similar to the observations in Tolosa, vegetation had re-established in the washover area within a very short period of time. Bioturbation likely disturbed the top layers, especially on top of the beach ridge (e.g., DOL 12, Fig. 9).

The stratigraphy of the first ridge was composed of a massive, moderately sorted and unimodal medium sand, rich in skeletal grains, with a mean grain size ranging between 250 and 375 µm. The grain size distribution of the fresh storm deposit was similar, though slightly coarser (Fig. 8, Fig. S9). Some horizons were darker due to the accumulation

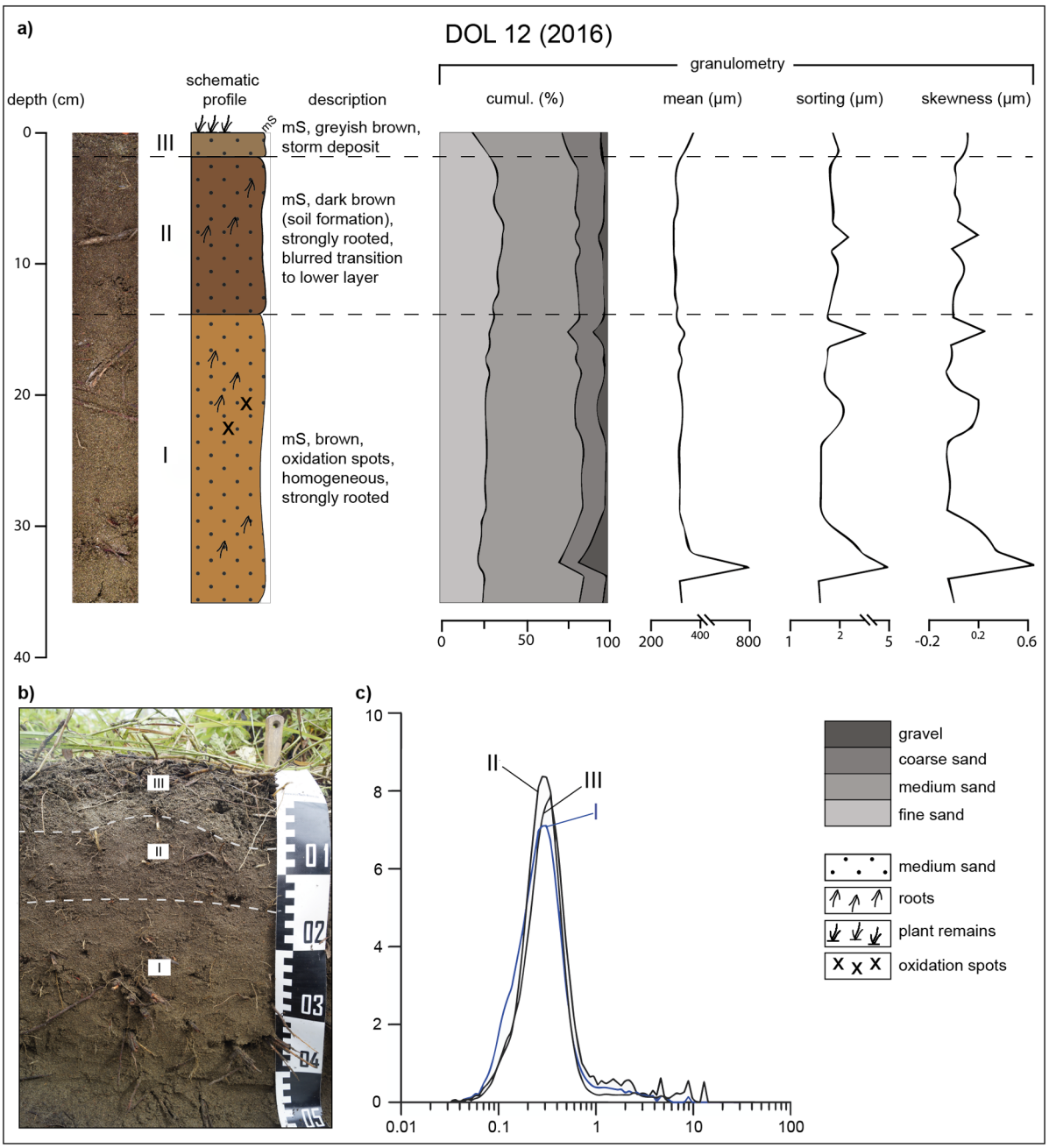

Fig. 9: Sedimentary characteristics of DOL 12 (2016). (a) The stratigraphic profile is characterised by strong root penetration and thus (b) by a blurred transition between the different layers. No significant differences of grain size parameters are apparent, but (c) grain size distribution reveals a slight shift to a finer grain size in Layer I.

of organic matter and showed a slight shift in mean grain size, for example in DOL 12 with 300 µm in Layer II compared to 330 µm in Layer I. DOL 15, is located in the first swale and showed the most intense soil formation as well as the lowest mean grain size (Fig. S11). In DOL 14, C and N contents of the sandy substrate were generally low at 0.15–0.18 % and 0.4–0.6 %, respectively, and only showed minor variations throughout the different layers. Higher C (0.2–0.3 %) and N (0.9–1.6 %) amounts were only measured in the dark brown coloured pre-Haiyan soil (Layer II), which was characterised by a slightly higher mud component and degree of bioturbation (Fig. 8).

4.1.3 Source of storm deposits

Offshore samples were taken down to water depths of 13.4 m at Tolosa and 10.7 m at Dolores (Fig. 10). At both sites, the samples showed a seaward fining trend and sorting became poorer with increasing distance to the shore (Fig. 10, Fig. 11). At Tolosa, mean grain size ranged from 246 µm at a distance of about 25 m to the shoreline and a water depth of 1.2 m to 33 µm at 480 m (in 13.4 m water depth). At depths of ≤4 m samples mainly consisted of sand, whereas the samples at >10 m water depth were less sorted and dominated by silt. At Dolores, the mean grain size ranged between 283 and 19 µm with a clear seaward fining trend. At 10 m offshore and at a depth of less than 1 m the mean grain size was below the one of the onshore storm deposits (DOLO 2 = 217 µm, onshore samples >250 µm) (Fig. 10, Fig. 11, Tab. S3). At both sites, the closer the samples were located to the shore, the greater was the similarity with the sandy typhoon deposits documented during the surveys (Fig. 11).

4.2 Shoreline change analysis

Along the relatively straight and even coastal stretch of 12 km around Tolosa, an average coastal retreat of 26 m was calculated after Typhoon Haiyan (Tab. S3), which is considered a minimum estimate as accretion of the coastline might have already started during the seven days between the typhoon and the image capture. The retreat was largest (35 m) where spits and barriers were eroded adjacent to small creeks and river mouths (Fig. 12). Following the erosive impact of the typhoon, the coastline started to recover to an average distance of 11 m from its pre-typhoon position in May 2015. The rates of recovery were highest in areas of strongest typhoon-induced erosion (up to 32 m), near the river mouths. In these areas, the shoreline almost reached its pre-Haiyan position. However, in some parts (17 out of 215 transects) an erosional trend continued until 2015 (Fig. 13a,b)

At Dolores, a more complex pattern of erosion and deposition was observed. At more than half of the transects (164 from 267 in total), the coastline had prograded by an average of 57 m six days after Typhoon Haiyan (Fig. 13a,c, Fig. 14, Tab. S4). The highest sediment accumulation occurred near the river mouths of the Dolores and Ulot rivers, the entrance of some smaller creeks and especially along the mangrove-fringed headland in the north of the investigated area (+73 m on average). Accumulation of sediment during the inundation of the typhoon seems to have formed new shoals and sand bars in these areas. In contrast, the beaches in between the

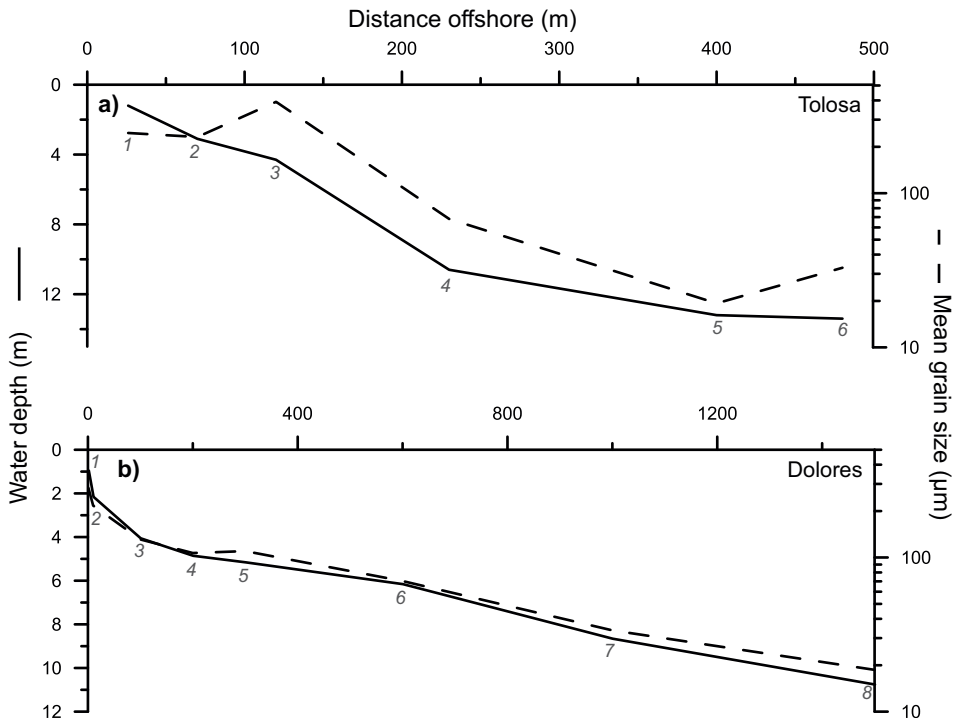

Fig. 10: Trend of mean grain size with offshore water depth at a) Tolosa and b) Dolores. Numbers indicate sample numbers as in Fig. 1b,c.

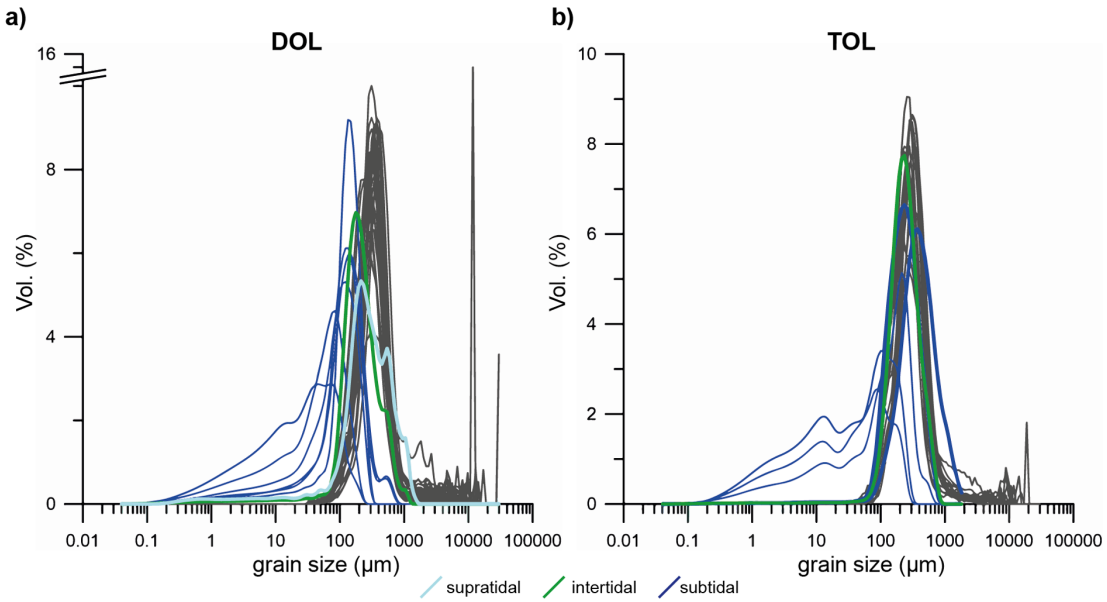

Fig. 11: Comparison of grain size distributions from the onshore storm deposits (dark grey) with offshore samples; (a) Dolores, (b) Tolosa

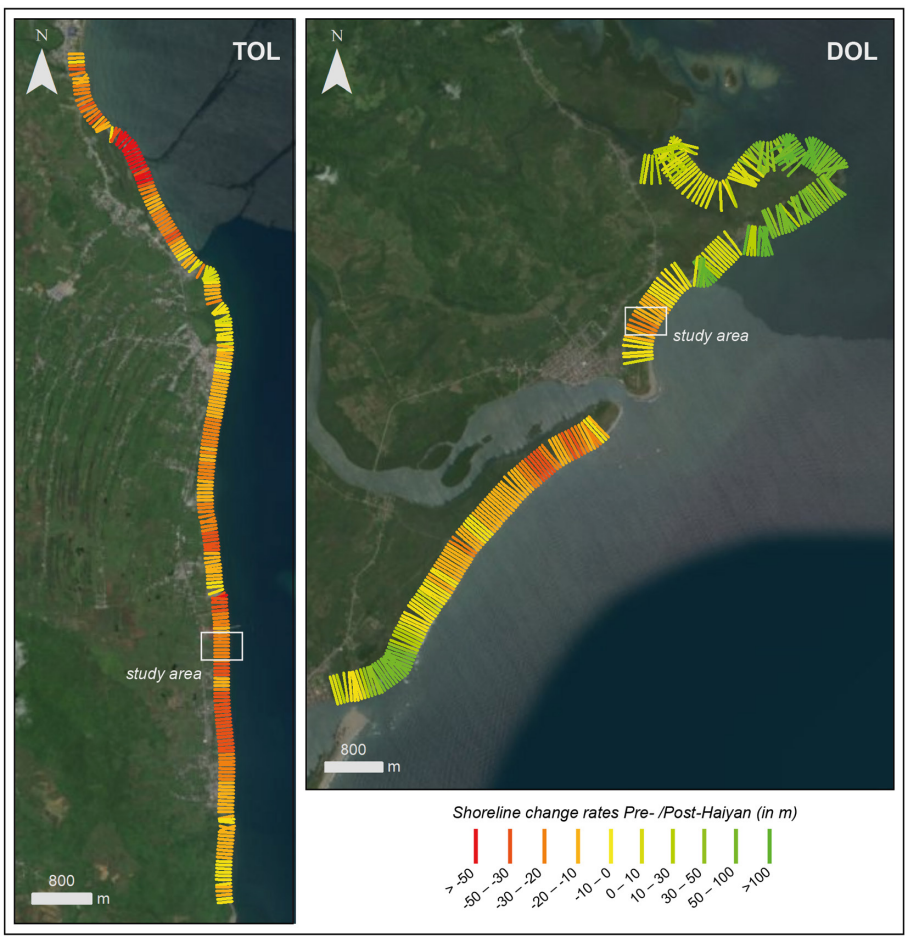

Fig. 12: Shoreline change rates following Typhoon Haiyan (basemap by ESRI)

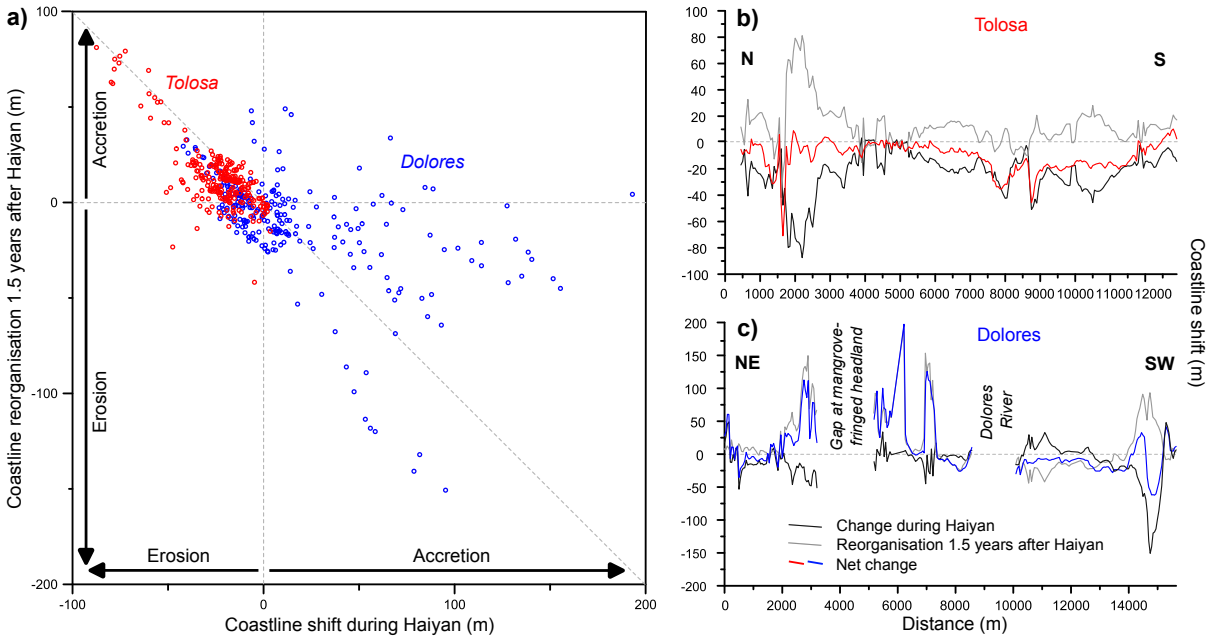

Fig. 13: Pattern of erosion and accretion during Typhoon Haiyan and 1.5 years after the event (recovery phase) based on the DSAS analysis. a) Biplot showing post-typhoon change vs. recovery phase for both study sites. b) Erosion and accretion along the Tolosa transect from N to S. c) Erosion and accretion along the Dolores transect from NE to SW (see Fig. 14).

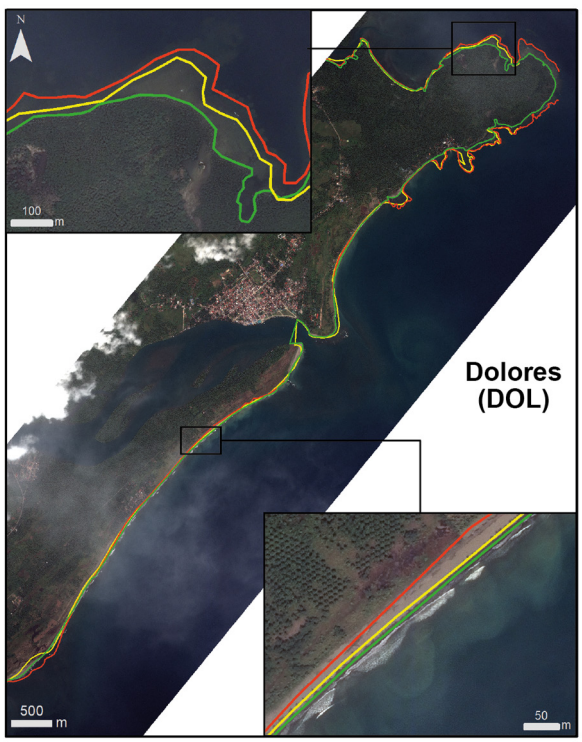

Fig. 14: Shoreline change at Dolores. (a) At the mangrove-covered headland in the north, net accumulation was detected following the impact of Typhoon Haiyan. The pre-Haiyan position of the shoreline was not reached until May 2015. (b) The coastline was eroded along an elongated beach, but recovery started rapidly after Haiyan. In May 2015 the pre-Haiyan shoreline position was nearly reached (see Tab. S1 for details on satellite images).

accretional areas experienced an average shoreline retreat of 15 m (Fig. 13a,c, 14, Tab. S4).

In the following months, erosion dominated over accretion at 161 out of 241 transects, whereby the areas with highest accretion immediately after the typhoon also experienced the strongest erosion until May 2015. Near the river mouths, on average 51 m of the previous accretion of 73 m were eroded again. Overall, a progressive alignment of the shoreline to its pre-Haiyan position was noticed along the entire coastal stretch. Nevertheless, the initial shoreline position was not reached in May 2015 and some of the new post-Haiyan shoals and sand bars remained unchanged over the studied period (Fig. 14).

5 Discussion

5.1 Geomorphic and sedimentological imprint of Typhoon Haiyan

At Tolosa, the majority of geomorphic effects can be related to Typhoon Haiyan, although some very limited modification of the proximal depositional patterns by Tropical Storm Basyang in February 2014 cannot be excluded (Brill et al. 2016). At Dolores, Typhoon Hagupit in December 2014 reached an intensity comparable to Haiyan, even though the majority of coastal flooding as well

as geomorphic and sedimentological effects can be associated with Typhoon Haiyan based on local eyewitness reports.

Outside of river mouths, sandy beaches experienced significant erosion and shoreline retreat of more than 35 m on average in both areas. These values, however, are smaller compared to other high-energy wave events such as Hurricane Katrina in 2005 (Fritz et al. 2007) or the Indian Ocean tsunami in 2004 (Liew et al. 2010, Monecke et al. 2015), where an initial shoreline retreat of 100–500 m was measured at the hardest-hit coastlines. At Tolosa, erosion was strongest in areas with high sediment input along the beaches and where protective sand bars in front of river mouths were removed during the typhoon. These trends are consistent with the results of other studies highlighting the high vulnerability of sandy beach sections to erosion as compared to other coastal landforms (Jonah et al. 2016).

The differential pattern of erosion and accretion during Haiyan at Dolores may be explained by connectivity to the offshore island of Hilabaan, where eyewitnesses reported massive erosion along the seaward facing beaches and complete inundation (3–4 m above msl) of the island (Quix 2018). Exposed roots of palm trees on Hilabaan island found in 2015 indicate vertical erosion of >20–30 cm (Fig. 8c) along the entire east coast. In addition to an increased amount of fluvial input during the typhoon due to heavy rains, these sediments were supposedly transported towards the mainland by storm waves coming from a south-easterly direction and were mainly trapped around the mangrove-fringed headland north of Dolores, reflected by the highest values of coastline accretion (Fig. 13c, 14).

At both study sites beaches were eroded by the storm waves, leaving an erosive scarp as a typical response (Wang et al. 2006, Yu et al. 2013). Flow depths of at least 4 m completely submerged the barrier crests with maximum heights of 3.3 m above msl and deposited sand on top of the beach ridge and inside the first swale. The landward-thinning and slightly fining sand sheet extends for approximately 150 m inland. In the back-barrier depression at Tolosa, a thick washover sand lobe with landward inclining laminae (Unit 2) is situated on top of the sand sheet (cf. Brill et al. 2016). At Dolores, the thickness of the storm deposit is also greatest on top and on the leeward side of the barrier, but the deposit appears massive and characteristic features such as a landward declining upper surface, a steep landward front or planar lamination patterns (Schwartz 1982, Kochel & Dolan 1986, Sedgwick & Davies 2003, Phantuwongraj et al. 2013, May et al. 2017) were not visible in 2015.

5.2 Spatial variability of typhoon signatures

The extent of beach erosion and deposition of washover sediments is influenced by several site-specific factors including storm intensity, approaching angle of the storm waves, wave height, local geology, coastal configuration, sediment texture and supply as well as the bathymetry of the study area (Coco et al. 2014, Burvingt et al. 2017, Moskalewicz et al. 2024). Although both locations have a different exposure to the typhoon track, a combination of exceptionally high waves and inundation levels caused beach erosion along both investigated coastal stretches. The almost shore-perpendicular approaching angle of the storm waves resulted in an almost evenly distributed, lateral erosion pattern in Tolosa, whereas the erosion in Dolores implies a more oblique angle towards north-northwest associated with predominant erosion at the beach and accretion towards the northeastern mangrove-fringed headland (Fig. 13c, Fig. 14, Fig. 15). These site-specific effects emphasise the strong influence of the approaching angle of waves and sediment connectivity (with Hilabaan) on beach response with the potential effect of increased longshore sediment transport after the event (Bergillos et al. 2017, Burvingt et al. 2017).

At both investigated sites, the deposition of sand sheets reached a similar landward extent (~150 m), connected to washover fans in the backshore. The sand sheets are related to a continuous flow of water over the entire crest and deposition from suspension (Donnelly et al. 2006). At Tolosa, breaking waves at the barrier during peak inundation created maximum suspended transport of >0.05 m^2/s contributing to the deposition of a washover fan (Unit 2) in the backshore and on top of the proximal sand sheet (Fig. 3a). However, shear stress reduced quickly inland after breaking of waves and, in combination with abundant vegetation increasing bottom roughness, resulted in the relatively short landward limit of sand deposition (Watanabe et al. 2017).

In contrast, a moderate storm surge occurred in Dolores, which is located more than 100 km north of the eye of the typhoon, due to the relatively steep offshore bathymetry (Tajima et al. 2016b). In case of Eastern Samar (Dolores) high flood levels resulted from extremely high waves (Bricker et al. 2014) eroding the beach. The high waves overtopped the beach ridge at Dolores and deposited a sand sheet on top of the first ridge reaching down into the swale. However, flooding intensity was probably less than in Tolosa as deposits are thinner and their thickness decreases much faster with greater distance to the shoreline.

At Dolores, the differentiation of storm deposits based on granulometric criteria is hampered by only minimal variations in grain size distribution and sorting compared to the underlying soil and the lack of lamination. Granulometric investigations of the offshore reference samples reveal that the main source area of the washover deposits comprised the beach and the supratidal beach, which explains the similarity between storm deposit and the sandy pre-typhoon soil. In contrast, the finer grained sand sheets in Tolosa not only stem from the beach area but also from the intertidal and very shallow subtidal environment. A mud component as documented by Soria et al. (2017) in more landward samples at Tanauan north of Tolosa may indicate sourcing of sediments at even greater depth, supported by the shallow and gently-sloped offshore bathymetry in combination with high flow depth and flow velocity (cf. Mori et al. 2014). At Dolores, high sediment availability in the beach zone (see section 5.1) as well as the higher crest of the barrier may point to only a small source component from the shallow subtidal. In general, these observations are in line with estimates of a beach/intertidal to very shallow subtidal or reef flat sediment source of onshore Haiyan deposits in the wider study area (Brill et al. 2016, Switzer et al. 2020).

Besides bathymetry, coastal configuration and sediment supply, the local composition of the typhoon deposits is influenced by the geological origin of the investigated areas. Laminated storm deposits are only present in the siliciclastic environment of Tolosa, but not at the carbonate-dominated coastline in Dolores as they are linked to the existence of heavy minerals and kinetic sieving (Brill et al. 2016, Soria et al. 2017).

Signs of shore-perpendicular breaches as reported elsewhere from both tsunamis (Atwater et al. 2013) and major storm (Stone et al. 2004, Wang & Briggs 2015, Baumann et al. 2017, May et al. 2017) impacts, the latter mostly associated with barrier islands, have not been identified in the study area as a response to Typhoon Haiyan.

5.3 Post-typhoon sedimentary and geomorphic changes

The post-typhoon beach dynamics were characterised by recovery towards the original state, at varying rates. At Tolosa, 91 % of the sediment initially lost to Typhoon Haiyan at the exposed areas of small river outlets was recovered in the months following the event. On average, the coastline recovered to more than half (58 %) of its pre-Haiyan position within 1.5 years (Fig. 14a,b, Tab. S3). Similar cases of rapid beach recovery were reported after impacts of both major storms and tsunamis (e.g., Wang et al. 2006, Choowong et al. 2009, Liew et al. 2010, Yu et al. 2013, Monecke et al. 2015). Usually, various phases of recovery can be distinguished over longer periods with very high lateral accretion rates in the first months and a subsequent slow down due to decreasing sediment supply (Yu et al. 2013, Monecke et al. 2015, Oliver 2016) until a state somewhere close to pre-impact conditions is reached. Anderson et al. (2010) emphasise that the sum of the discrepancy between the pre-impact and recovery states (transient change) determines the long-term dynamics (persistent change) of a low-lying sand-ridge coast.

Since accretion was most pronounced in areas with high sediment supply, the availability of material for beach progradation also seemed to be one of the driving factors for coastal recovery in Tolosa. Typhoon-eroded sand was transported back to the beach within a short time interval by long-term wave action and longshore drift as also described for sandy beaches in Hong Kong by Yu et al. (2013). Only where long-term wave energy is too low (Yu et al. 2013), anthropogenic overprint is severe (e.g. in case of fish tanks inside wetlands behind an eroded sand barrier; Liew et al. 2010), or the eroded beach deposits are transported to greater depths below the storm wave base by backwash, as in the case of the 2011 Tohoku Tsunami inside Sendai Bay (Yoshikawa et al. 2015), post-impact recovery fails.

At Dolores (Fig. 15), sediment was kept within reach of the long-term wave climate resulting in net erosion where Typhoon Haiyan had induced accretion, whereas areas of beach loss gained sediment in the months after the typhoon. In fact, both study sites benefit from shallow water depths (Fig. 10) close to the coast in the Gulf of Leyte (Fig. 1a) and the lee of Hilabaan Island (Fig. 15). Under such conditions, several studies along the European Atlantic coast and in the Gulf of Mexico show that despite site-specific variability in erosion and accretion during storm impacts, beaches tend to recover towards some sort of pre-storm equilibrium (Stone et al. 2004, Coco et al. 2014, Masselink et al. 2015, Scott et al. 2016, Burvingt et al. 2017), which may take up to >10 years in extreme cases (Kümmerer et al. 2025).

Furthermore, the total amount of eroded, accumulated and later redistributed sediment after the storm was significantly larger in Dolores compared to Tolosa. Nevertheless, coastal recovery remained

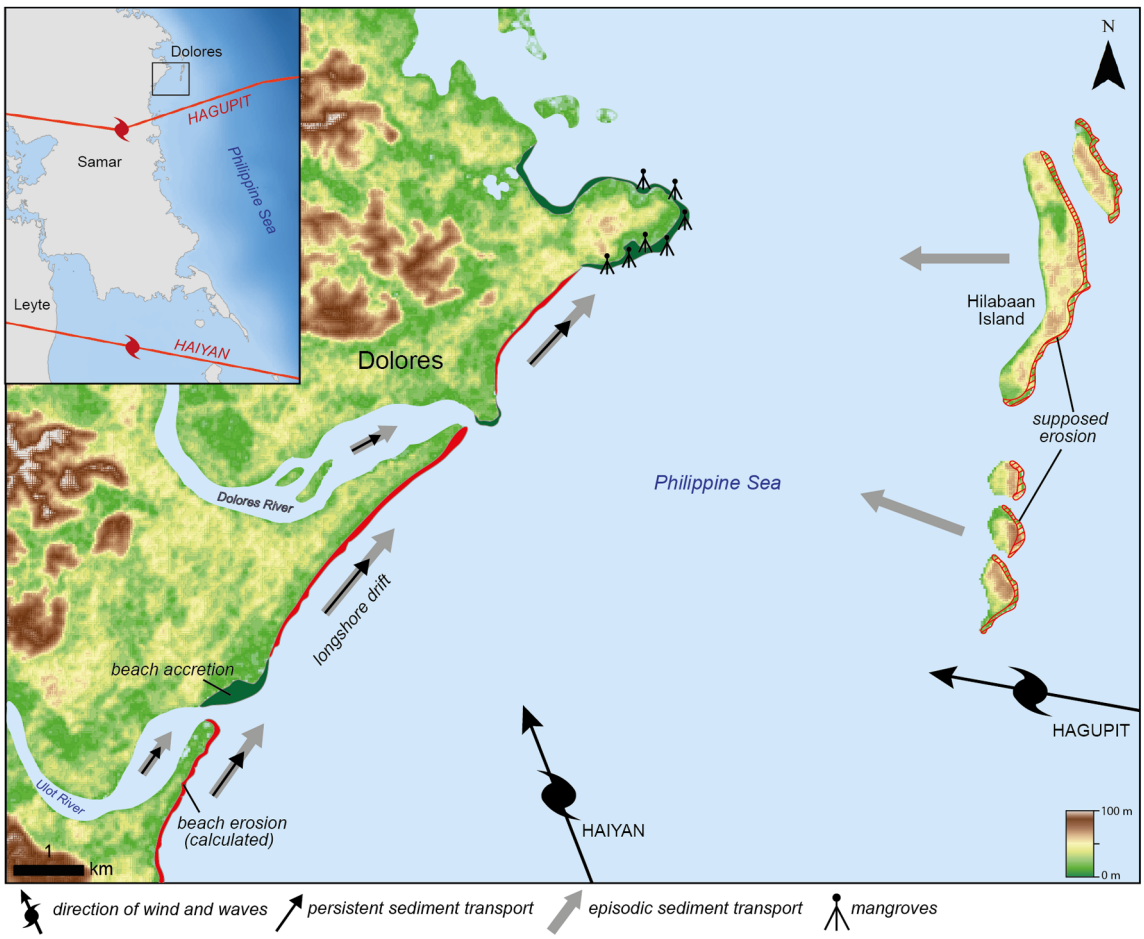

Fig. 15: Supposed processes affecting coastal change in Dolores. Regular sediment movement due to longshore drift currents and fluvial input was intensified during Typhoon Haiyan leading to a general shoreline change pattern of both erosion (red) and accretion (green) (based on ESRI base maps and SRTM data from USGS).

behind the pre-Haiyan shoreline position, especially in areas were new sandbars were formed. Although erosion outweighed accretion in the months following the typhoon, most of the new sandbars still existed on the 2015 satellite images. We assume that recovery processes were interrupted or at least negatively affected by a higher number of potentially erosive storms recurring in subsequent months such as Typhoon Hagupit (December 2014) and Tropical Storm Mekkhala (January 2015). Consequently, sediment reorganisation and net shoreline accretion can be attributed to the reestablishment of long-term coastal processes such as longshore drift during regular wave action as well as reintegration of offshore transported sediment and the frequency of major storm impacts (e.g., Stone et al. 2004, Burvingt et al. 2017). Whether Typhoon Haiyan induced transfer from lower to upper shoreface environments and increased the sediment budget available for long-term shoreline accretion potential compensation of relative sea-level rise (Harley et al. 2022) cannot be evaluated based on the short recovery phase covered by this study.

On a smaller spatial scale, sediment accretion impacts the beach profile by transferring sediment from the upper intertidal area to the beach face by wave action rebuilding the eroded beach ridge. Since the formation of ridges is restricted to areas of rapid accretion, dense vegetation and accumulation of sediment at the foot of the storm-induced scarp (Hesp et al. 2005), the local conditions at Tolosa promoted the rapid establishment of a new berm as shown in Fig. 2d. Thus, wherever sediments remain in the nearshore system, coasts seem to recover without human intervention after extreme-wave impact. Hence, the recommended management of these natural coastlines is to leave them to reorganise by themselves (Liew et al. 2010).

Vegetation growth plays a major role in attenuating flooding, sediment deposition (Watanabe et al. 2017) and coastal recovery processes through the stabilising effects of roots and trapping aeolian sand (Engel et al. 2015, Monecke et al. 2015). At both sites, ground covering plants – in particular *Ipomoea* – spread on top of the eroded ridge within a very short time and kept up with the pace of beach progradation. Their roots, however, in combination with fast weathering driven by a high amount of rainfall and good drainage (Navarrete et al. 2008), induced a disturbance of the laminated storm deposit and mixing with the underlying surrounding (incipient) soil (Fig. 2a–c, Fig. 4), which is reflected by a poorer sorting of the corresponding sand layers. At Dolores, the bioturbation process was reinforced by chemical weathering in the carbonate environment, which initiated soil formation processes. In the course of incipient soil formation, particles were geochemically altered, which is manifested by weathering attributes and a slight reduction of particle size over time (e.g., DOL 12, DOL 15).

5.4 Implications for coastal geomorphic resilience after extreme events

The sedimentary and geomorphic record of beach-ridge systems has important implications for the reconstruction of coastline evolution and the history of extreme-wave impacts. Even though the preservation potential of sandy beach ridges is reduced compared to ridges composed of coarse clasts (Scheffers et al. 2012), they have been successfully used to decipher prehistoric events or even variability in storminess (e.g., Tamura 2012, Brill et al. 2015, Monecke et al. 2015, Nott et al. 2015, Oliver 2016, Oliver et al. 2019, May et al. 2018). Observations of the geomorphic response of these systems made after the impact of Typhoon Haiyan help us to read them as a long-term archive for storminess.

Based on remnants of plastic trash found down to depths of 50 cm at the erosive scarp at Dolores (DOL 9, DOL 14) the age of the most seaward ridge is assumed to be post-World War II, when the use of synthetic polymers started to spread globally to become a distinct stratigraphic time marker (Zalasiewicz et al. 2014). This young age poses the question of the preservation potential of Haiyan's geomorphic imprint. Liew et al. (2010) state that coastal morphology is not an ideal indicator for past events as recovery processes mask the erosive signature after only a few weeks to months. Such a masking process has occurred already at Tolosa and, to a lesser degree, at Dolores, where recovery was certainly slowed down by subsequent typhoons. However, at prograding barrier coasts, former scarps can often be detected and dated by a combination of ground penetrating radar (GPR) and optically stimulated luminescence (OSL) dating and translated into millennial-scale records of storminess (Tamura 2012, Oliver 2016, Dougherty et al. 2019, Kumar et al. 2024). While the application of GPR would be promising in future activities at the study sites, the application of OSL is challenging, as luminescence signals of the young volcanic quartz sands of Leyte have been found to be poor and feldspars were insensitive to infrared stimulation (Brill et al. 2018).

In light of the relatively high level of geomorphic resilience, the preservation potential of washover sand sheets and fans at both sites is considered poor on the basis of the results presented. At least in the Philippines' humid tropical climate, rapid reestablishment of vegetation, bioturbation and incipient soil formation processes (accumulation and percolation of organic matter, rapid weathering of less resistant minerals), signatures are either overprinted by post-depositional processes, as observed in both siliclastic and carbonate-dominated deposits of the 2004 Indian Ocean Tsunami (Nichol & Kench 2008, Szczuciński 2020) or destroyed by erosion of subsequent storms. However, there may be a chance to detect palaeo-surfaces reflected by incipient soil formation (e.g. DOL 9), which has been successfully used in a large overwash fan at the Gulf of Exmouth, Western Australia, to identify alternating phases of increased storm overwash and surface stability (May et al. 2017).

Where storm deposits have the same source material as the underlying substrate (e.g. in Dolores), their identification is further impeded and may be impossible due to bioturbation. This applies particularly to very thin sand layers, which in general have a very low likelihood of being preserved (Otvos 2011).

6 Conclusions

Typhoon Haiyan's impact on the two sites on Leyte and Samar comprised beach erosion as well as the deposition of a storm deposit on the most seaward, partly eroded beach ridge and inside the adjacent swale. These storm-related signatures such as an erosive scarp at the seaward side of the ridge, landward fining sand sheets and a laminated washover fan (Tolosa) are characteristic signatures of ty-

phoon impact. Since they were generated by one of the strongest tropical cyclones on record they represent an important contribution to the general knowledge on sedimentological storm signatures and their post-event alteration. However, preservation potentials are rather poor, as less than two years after the typhoon characteristic sedimentary structures, such as planar lamination, have been largely destroyed by bioturbation and weathering in the humid-tropical environment. The comparison of Haiyan's footprint at two different locations emphasises the influence of site-specific factors on both formation and preservation of erosional and depositional patterns, such as approaching angle and height of the waves, storm surge, local geology, coastal topography and sediment texture.

The findings of this study point to a fast recovery after typhoon impact closely approaching pre-typhoon conditions in major parts of the studied coastline, especially at Tolosa, which has important implications for coastal management. The pattern is more complex at Dolores, where the coastline is disrupted by river mouths and has experienced a higher frequency of stronger storms in the wake of Haiyan. The indifferent reorganisation is controlled by constant wave action, longshore currents, sediment supply and vegetation growth. Within the beach ridge systems erosive scarps, existing sand deposits and typical storm-induced sediment structures were modified by intense bioturbation and incipient soil formation. Although post-depositional alterations in beach ridge systems are site dependent, in the humid and bioturbation intense coastal environment of Eastern Visayas typhoon signature preservation is not sufficient to allow an easy detection. Their function as geological archive for past extreme-wave impacts is therefore considered limited at this stage of investigation.

Acknowledgements

This study was financially supported by the Faculty of Mathematics and Natural Sciences, University of Cologne (UoC), and by a UoC Postdoc grant awarded to Max Engel (ZUK 81/1) as part of the excellence initiative of the German federal and state governments. Invaluable administrative and logistic support was provided by Project NOAH (Nationwide Operational Assessment of Hazards), now the NOAH Center of the University of the Philippines' Resilience Institute, in particular Alfredo Mahar Francisco Lagmay and John Kenneth Suarez. We are grateful to the whole storm surge team of Project NOAH for hosting Eva Quix during a graduate internship in 2015. Laboratory analyses were supported by Stephan Opitz. Shoreline analysis with ArcGIS benefited from the expertise of Andreas Bolten (both UoC). Finally, we gratefully acknowledge two anonymous reviewers whose constructive comments substantially improved the manuscript.

References

Anderson TR, Frazer LN, Fletcher CH (2010) Transient and persistent shoreline change from a storm. *Geophysical Research Letters* 37: L08401. https://doi.org/10.1029/2009GL042252

Atwater BF, Cisternas M, Yulianto E, Prendergast AL, Jankaew K, Eipert AA, Fernando WIS, Tejakusuma I, Schiappacasse I, Sawai Y (2013) The 1960 tsunami on beach-ridge plains near Maullín, Chile: Landward descent, renewed breaches, aggraded fans, multiple predecessors. *Andean Geology* 40: 393–418.

Aurelio MA, Pena RE (2002) The geology and mineral resources of the Philippines. Volume 1: Geology. Manila.

Baumann J, Chaumillon E, Bertin X, Schneider J-L, Guillot B, Schmutz B (2017) Importance of infragravity waves for the generation of washover deposits. *Marine Geology* 391: 20–35. https://doi.org/10.1016/j.margeo.2017.07.013

Bergillos RJ, Masselink G, Ortega-Sánchez M (2017) Coupling cross-shore and longshore sediment transport to model storm response along a mixed sand-gravel coast under varying wave directions. *Coastal Engineering* 129: 93–104. https://doi.org/10.1016/j.coastaleng.2017.09.009

Bird ECF (ed) (2010) Philippines. *Encyclopedia of the world's coastal landforms:* 1151–1156. Dordrecht. https://doi.org/10.1007/978-1-4020-8639-7_214

Blott SJ, Pye K (2001) GRADISTAT: A grain size distribution and statistics package for the analysis of unconsolidated sediments. *Earth Surface Processes and Landforms* 26: 1237–1248. https://doi.org/10.1002/esp.261

Bricker J, Takagi H, Mas E, Kure S, Adriano B, Yi C, Roeber V (2014) Spatial variation of damage due to storm surge and waves during Typhoon Haiyan in the Philippines. *Journal of Japan Society of Civil Engineers, Series B2* 70: 231–235. https://doi.org/10.2208/kaigan.70.I_231

Brill D, Jankaew K, Brückner H (2015) Holocene evolution of Phra Thong's beach-ridge plain (Thailand) – Chronology, processes and driving factors. *Geomorphology* 245: 117–134. https://doi.org/10.1016/j.geomorph.2015.05.035

Brill D, May SM, Engel M, Reyes M, Pint A, Opitz S, Dierick M, Gonzalo LA, Esser S, Brückner H (2016) Typhoon Haiyan's sedimentary record in coastal environments of the Philippines and its palaeotempestological implications. *Natural Hazards and Earth System Sciences* 16: 2799–2822. https://doi.org/10.5194/nhess-2016-224.

Brill D, Reimann T, Wallinga J, May SM, Engel M, Riedesel S, Brückner H (2018) Are feldspar single-grains suitable for luminescence dating of late Holocene cyclone and tsunami deposits? *Quaternary Geochronology* 48: 91–103. https://doi.org/10.1016/j.quageo.2018.09.001

Burvingt O, Masselink G, Russell P, Scott T (2017) Classification of beach response to extreme storms. *Geomorphology* 295: 722–737. https://doi.org/10.1016/j.geomorph.2017.07.022

Choowong M, Phantuwongraj S, Charoentitirat T, Chutakositkanon V, Yumuang S, Charusiri P (2009) Beach recovery after 2004 Indian Ocean tsunami from Phang-nga, Thailand. *Geomorphology* 104: 134–142. https://doi.org/10.1016/j.geomorph.2008.08.007

Coco G, Senechal N, Rejas A, Bryan KR, Capo S, Parisot JP, Brown JA, MacMahan JHM (2014) Beach response to a sequence of extreme storms. *Geomorphology* 204: 493–501. https://doi.org/10.1016/j.geomorph.2013.08.028

Donnelly C, Kraus N, Larson M (2006) State of knowledge on measurement and modeling of coastal overwash. *Journal of Coastal Research* 22: 965–991. https://doi.org/10.2112/04-0431.1

Dougherty AJ (2014) Extracting a record of Holocene storm erosion and deposition preserved in the morphostratigraphy of a prograded coastal barrier. *Continental Shelf Research* 86: 116–131. https://doi.org/10.1016/j.csr.2013.10.014

Dougherty AJ, Choi J, Turney CM, Dosseto A (2019) Technical note: Optimizing the utility of combined GPR, OSL, and Lidar (GOaL) to extract paleoenvironmental records and decipher shoreline evolution. *Climate of the Past* 15: 389–404. https://doi.org/10.5194/cp-15-389-2019

Engel M, May SM, Scheffers A, Squire P, Pint A, Kelletat D, Brückner H (2015) Prograded foredunes of Western Australia's macro-tidal coast – Implications for Holocene sea-level change and high-energy wave impacts. *Earth Surface Processes and Landforms* 40: 726–740. https://doi.org/10.1002/esp.3663

Flater D (1998) WXTide32. http://wxtide32.com (last access: 14th Feb 2025).

Folk RL, Ward WC (1957) Brazos River Bar: A study in the significance of grain size parameters. *Journal of Sedimentary Petrology* 27: 3–26. https://doi.org/10.1306/74D70646-2B21-11D7-8648000102C1865D

Fritz HM, Blount C, Sokoloski R, Singleton J, Fuggle A, McAdoo BG, Moore A, Grass C, Tate B (2007) Hurricane Katrina storm surge distribution and field observations on the Mississippi Barrier Islands. *Estuarine, Coastal and Shelf Science* 74: 12–20. https://doi.org/10.1016/j.ecss.2007.03.015

García-Rubio G, Huntley D, Kingston K, Esteves L (2009) Shoreline identification using satellite images. *Proceedings of Coastal Dynamics* 2009: 117. https://doi.org/10.1142/9789814282475_0117

GEBCO Compilation Group (2024) GEBCO 2024 Grid. https://doi.org/10.5285/1c44ce99-0a0d-5f4f-e063-7086abc0ea0f

Hapke CJ, Himmelstoss EA, Kratzmann MG, List JH, Thieler ER (2011) National assessment of shoreline change: Historical shoreline change along the New England and Mid-Atlantic coasts. *USGS Open-File Report* 2010-1118. https://doi.org/10.3133/ofr20101118

Harley MD, Masselink G, Ruiz de Alegría-Arzaburu A, Valiente NG, Scott T (2022) Single extreme storm sequence can offset decades of shoreline retreat projected to result from sea-level rise. *Communications Earth & Environment* 3: 112. https://doi.org/10.1038/s43247-022-00437-2

Hesp P, Dillenburg S, Barboza E, Tomazelli LJ, Ayup-Zouain RN, Esteves LS, Gruber NLS, Toldo Jr EE, Tabajara LLCDA, Clerot LCP (2005) Beach ridges, foredunes or transgressive dunefields? Definitions and an examination of the Torres to Tramandai barrier system, Southern Brazil. *Anais da Academia Brasileira de Ciências* 77: 493–508. https://doi.org/10.1590/S0001-37652005000300010

Jonah FE, Boateng I, Osman A, Shimba MJ, Mensah EA, Adu-Boahen K, Chuku EO, Effah E (2016) Shoreline change analysis using end point rate and net shoreline movement statistics: An application to Elmina, Cape Coast and Moree section of Ghana's coast. *Regional Studies in Marine Sciences* 7: 19–31. https://doi.org/10.1016/j.rsma.2016.05.003

Knapp KR, Kruk MC, Levinson DH, Diamond HJ, Neumann CJ (2010) The international Best Track Archive for Climate Stewardship (IBTrACS): Unifying tropical cyclone data. *Bulletin of the American Meteorological Society* 91: 363–376. https://doi.org/10.1175/2009BAMS2755.1

Kochel RC, Dolan R (1986) The role of overwash on a mid-Atlantic coast barrier island. *Journal of Geology* 94: 902–906. https://doi.org/10.1086/629096

Kumar R, Switzer AD, Gouramanis C, Bristow CS, Shaw TA, Jankaew K, Li T, Brill D (2024) Late-Holocene sea-level markers preserved in a beach ridge system on Phra Thong Island, Thailand. *Geomorphology* 465: 109405. https://doi.org/10.1016/j.geomorph.2024.109405

Kümmerer V, Ferreira Ó, Loureiro C (2025) Distinct shoreline behaviour along storm-dominated and geologically controlled coastal barriers. *Earth Surface Processes and Landforms* 50: e70042. https://doi.org/10.1002/esp.70042

Lagmay AMF, Tejada MLG, Pena RE, Aurelio MA, Davy B, David S, Billedo E (2009) New definition of Philippine plate boundaries and implications to the Philippine Mobile Belt. *Journal of the Geological Society of the Philippines* 64: 17–30.

Lagmay AMF, Agaton RP, Bahala MAC, Briones JBLT, Cabacaba KMC, Caro CVC, Dasallas LL, Gonzalo LAL, Ladiero CN, Lapidez JP, Mungcal MTF, Puno JVR, Ramos MMAC, Santiago J, Suarez JK, Tablazon JP (2015) Devastating storm surges of Typhoon Haiyan. *International Journal of Disaster Risk Reduction* 11: 1–12. https://doi.org/10.1016/j.ijdrr.2014.10.006

Lapidez JP, Tablazon J, Dasallas L, Gonzalo LA, Cabacaba KM, Ramos MMA, Suarez JK, Santiago J, Lagmay AMF, Malano V (2015) Identification of storm surge vulnerable areas in the Philippines through the simulation of Typhoon Haiyan-induced storm surge levels over historical storm tracks. *Natural Hazards and Earth System Sciences* 15: 1473–1481. https://doi.org/10.5194/nhess-15-1473-2015

Leszczyńska K, Alexanderson H, Clemmensen L, Giza A, Lorenz S, Moskalewicz D, Oliński P, Paprotny D, Rosentau A, Rutgersson A, Stattegger K, Szczuciński W, Terefenko P, Uścinowicz G, Uścinowicz S, Wolski T (2025) A review of storms and marine coastal flooding in the Baltic Sea – Insights from instrumental, historical and sedimentary record. *Earth-Science Reviews* 266: 105137. https://doi.org/10.1016/j.earscirev.2025.105137

Liew SC, Gupta A, Wong PP, Kwoh LK (2010) Recovery from a large tsunami mapped over time: The Aceh coast, Sumatra. *Geomorphology* 114: 520–529. https://doi.org/10.1016/j.geomorph.2009.08.010

Lipakis M, Chrysoulakis N, Kamarianakis Y (2008) Shoreline extraction using satellite imagery. Pranzini E, Wetzel L (eds) *Beach Erosion Monitoring. Results from BEACHMED/e-OpTIMAL Project (Optimization des Techniques Integrées de Monitorage Appliquées aux Littoraux) INTERREG IIIC:* 81–95. Florence.

Maeda Y, Siringan F, Omura A, Berdin R, Hosono Y, Atsumi S, Nakamura T (2004) Higher-than-present Holocene mean sea levels in Ilocos, Palawan and Samar, Philippines. *Quaternary International* 115–116: 15–26. https://doi.org/10.1016/S1040-6182(03)00093-4

Mas E, Bricker J, Kure S, Adriano B, Yi C, Suppasri A, Koshimura S (2015) Field survey report and satellite image interpretation of the 2013 Super Typhoon Haiyan in the Philippines. *Natural Hazards and Earth System Sciences* 15: 505–816. https://doi.org/10.5194/nhess-15-805-2015

Masselink G, Hughes MG, Knight J (2011) Introduction to coastal processes and geomorphology. Cambridge.

Masselink G, Scott T, Poate T, Russell P, Davidson M, Conley D (2016) The extreme 2013/2014 winter storms: hydrodynamic forcing and coastal response along the southwest coast of England. *Earth Surface Processes and Landforms* 41: 378–391. https://doi.org/10.1002/esp.3836

May SM, Engel M, Brill D, Squire P, Scheffers A, Kelletat D (2013) Coastal hazards from tropical cyclones and extratropical winter storms based on Holocene storm chronologies. Finkl C (ed) *Coastal hazards:* 557–585. Dordrecht. https://doi.org/10.1007/978-94-007-5234-4_20

May SM, Brill D, Leopold M, Callow N, Engel M, Scheffers A, Opitz S, Norpoth M, Brückner H (2017) Chronostratigraphy and geomorphology of washover fans in the Exmouth Gulf (NW Australia) – a record of tropical cyclone activity during the late Holocene. *Quaternary Science Reviews* 169: 65–84. https://doi.org/10.1016/j.quascirev.2017.05.023

May SM, Gelhausen H, Brill D, Callow N, Engel M, Opitz S, Scheffers A, Joannes-Boyau R, Leopold M, Brückner H (2018) Chenier-type ridges in Giralia Bay (Exmouth Gulf, Western Australia) – Processes, chronostratigraphy, and significance for recording past tropical cyclones. *Marine Geology* 396: 186–204. https://doi.org/10.1016/j.margeo.2017.03.005

Minamidate K, Goto K (2024) Unveiling the history and nature of paleostorms in the Holocene. *Earth-Science Reviews* 253: 104774. https://doi.org/10.1016/j.earscirev.2024.104774

Monecke K, Templeton CT, Finger W, Houston BL, Luthi SM, McAdoo BG, Meilianda E, Storms JEA, Walstra D-J, Amna R, Hood N, Karmanocky FJ, Nurjanah, Rusydy I, Sudrajat SU (2015) Beach ridge patterns in West Aceh, Indonesia, and their response to large earthquakes along the Northern Sunda Trench. *Quaternary Science Reviews* 113: 159–170. https://doi.org/10.1016/j.quascirev.2014.10.014

Monecke K (2020) Erosional signatures and reorganization in ridge-and-swale sequences. Engel M, Pilarczyk J, May SM, Brill D, Garrett E (eds) *Geological records of tsunamis and other extreme waves:* 471–489. Amsterdam. https://doi.org/10.1016/B978-0-12-815686-5.00022-5

Mori N, Kato M, Kim S, Mase H, Shibutani Y, Takemi T, Tsuboki K, Yasuda T (2014) Local amplification of storm surge by Super Typhoon Haiyan in Leyte Gulf. *Geophysical Research Letters* 41: 5106–5113. https://doi.org/10.1002/2014GL060689

Morton RA, Miller TL, Moore LJ (2004) National assessment of shoreline change: Part 1, Historical shoreline changes and associated coastal land loss along the U.S. Gulf of Mexico. *USGS Open-File Report* 2004-1043. https://doi.org/10.3133/ofr20041043

Moskalewicz D, Bahr F, Janowski Ł, Leszczyńska K, Sitkiewicz P, Słowik M, Stattegger K, Tysiąc P, Winter C (2024) Morphology and internal structure of small-scale washovers formed in the coastal zone of the semi-enclosed tideless basin, Gulf of Gdańsk, Baltic Sea. *Geomorphology* 463: 109368. https://doi.org/10.1016/j.geomorph.2024.109368

Mühr B, Bessel T, Girard T, Brink SA, Khazai B, Kunz-Plapp T (2014) TYPHOON 22W "Hagupit" – Short Summary. Karlsruhe. https://www.cedim.kit.edu/download/CEDIM_hagupit2014_short.pdf (last access: 14th Feb 2025).

Navarrete IA, Tsutsuki K, Kondo R, Asio VB (2008) Genesis of soils across a late Quaternary volcanic landscape in the humid tropical island of Leyte, Philippines. *Australian Journal of Soil Research* 46: 403–414. https://doi.org/10.1071/SR08012

NDRRMC (National Disaster Risk Reduction and Management Council) (2014a) Final report re: Effects of tropical depression "AGATON". https://reliefweb.int/report/philippines/ndrrmc-update-final-report-re-effects-tropical-depression-agaton (last access: 18th Feb 2025)

NDRRMC (National Disaster Risk Reduction and Management Council) (2014b) SitRep No. 09 re: Effects of tropical storm "BASYANG" (KAJIKI). https://reliefweb.int/report/philippines/ndrrmc-update-sitrep-no-09-re-effects-tropical-storm-basyang-kajiki (last access: 18th Feb 2025)

Nichol SL, Kench PS (2008) Sedimentology and preservation potential of carbonate sand sheets deposited by the December 2004 Indian Ocean tsunami: South Baa atoll, Maldives. *Sedimentology* 55: 1173–1187. https://doi.org/10.1111/j.1365-3091.2007.00941.x

Nott J, Forsyth A, Rhodes E, O'Grady D (2015) The origin of centennial- to millennial-scale chronological gaps in storm emplaced beach ridge plains. *Marine Geology* 367: 83–93. https://doi.org/10.1016/j.margeo.2015.05.011

OCHA Philippines (2014) Typhoon Hagupit – Situation Report No. 3 (as of 8 December 2014). https://www.unocha.org/publications/report/philippines/philippines-typhoon-hagupit-situation-report-no-3-8-december-2014 (last access 11th Aug 2015).

Oliver TSN (2016) Holocene depositional history of three coastal sand ridge plains, southeastern Australia. PhD thesis, University of Wollongong, Australia.

Oliver TSN, Tamura T, Short AD, Woodroffe CD (2019) Rapid shoreline progradation followed by vertical foredune building at Pedro Beach, southeastern Australia. *Earth Surface Processes and Landforms* 44: 655–666. https://doi.org/10.1002/esp.4510

Otvos EG (2011) Hurricane signatures and landforms—toward improved interpretations and global storm climate chronology. *Sedimentary Geology* 239: 10–22. https://doi.org/10.1016/j.sedgeo.2011.04.014

PAGASA (Philippine Atmospheric, Geophysical and Astronomical Service Administration) (2025a) Climate of the Philippines. https://www.pagasa.dost.gov.ph/information/climate-philippines (last access: 14th Feb 2025).

PAGASA (Philippine Atmospheric, Geophysical and Astronomical Service Administration) (2025b) Climatological normals. https://www.pagasa.dost.gov.ph/climate/climatological-normals (last access: 14th Feb 2025).

PAGASA (Philippine Atmospheric, Geophysical and Astronomical Service Administration) (2025c) Philippine Area of Responsibility. https://www.pagasa.dost.gov.ph/learning-tools/philippine-area-of-responsibility (last access: 15th Jul 2025).

PAGASA (Philippine Atmospheric, Geophysical and Astronomical Service Administration) (2025d) Tropical cyclone information. https://www.pagasa.dost.gov.ph/climate/tropical-cyclone-information (last access: 17th Jul 2025).

Pajak MJ, Leatherman S (2002) The high water line as shoreline indicator. *Journal of Coastal Research* 18: 329–337.

Phantuwongraj S, Choowong M, Nanayama F, Hisada KI, Charusiri P, Chutakositkanon V, Pailoplee S, Chabangbon A (2013) Coastal geomorphic conditions and styles of storm surge washover deposits from Southern Thailand. *Geomorphology* 192: 43–58. https://doi.org/10.1016/j.geomorph.2013.03.016

Quix E (2018) Typhoon Haiyan's impact on beach ridge systems of the Eastern Visayas (Philippines) and their recovery potential. Master thesis, Institute of Geography, University of Cologne.

Ramos NT, Tsutsumi H (2010) Evidence of large prehistoric offshore earthquakes deduced from uplifted Holocene marine terraces in Pangasinan Province, Luzon Island, Philippines. *Tectonophysics* 495: 145–158. https://doi.org/10.1016/j.tecto.2010.08.007

Roeber V, Bricker J (2015) Destructive tsunami-like wave generated by surf beat over a coral reef during Typhoon Haiyan. *Nature Communications* 6: 7854. https://doi.org/10.1038/ncomms8854

Ruggiero P, Kratzmann MG, Himmelstoss EA, Reid D, Allan J, Kaminski G (2013) National assessment of shoreline change: Historical shoreline change along the Pacific northwest coast. *USGS Open-File Report* 2012–1007. https://doi.org/10.3133/ofr20121007

Scheffers A, Engel M, Scheffers S, Squire P, Kelletat D (2012) Beach ridge systems – archives for Holocene coastal events? *Progress in Physical Geography* 36: 5–37. https://doi.org/10.1177/0309133311419549

Schwartz RK (1982) Bedform and stratification characteristics of some modern smallscale washover sand bodies. *Sedimentology* 29: 835–849. https://doi.org/10.1111/j.1365-3091.1982.tb00087.x

Scott T, Masselink G, O'Hare T, Saulter A, Poate T, Russell P, Davidson M, Conley D (2016) The extreme 2013/2014 winter storms: Beach recovery along the southwest coast of England. *Marine Geology* 382: 224–241. https://doi.org/10.1016/j.margeo.2016.10.011

Sedgwick PE, Davis Jr RA (2003) Stratigraphy of washover deposits in Florida: implications for recognition in the stratigraphic record. *Marine Geology* 200: 31–48. https://doi.org/10.1016/S0025-3227(03)00163-4

Shimozono T, Tajima Y, Kennedy AB, Nobuoka H, Sasaki J, Sato S (2015) Combined infragravity wave and sea-swell runup over fringing reefs by super typhoon Haiyan. *Journal of Geophysical Research: Oceans* 120: 4463–4486. https://doi.org/10.1002/2015JC010760

Soria JLA, Switzer AD, Villanoy CL, Fritz HM, Bilgera PHT, Cabrera OC, Siringan FP, Yacat-Sta Maria Y, Ramos RD, Fernandez IQ (2016) Repeat storm surge disasters of Typhoon Haiyan and its 1897 predecessor in the Philippines. *Bulletin of the American Meteorological Society* 97: 31–48. https://doi.org/10.1175/BAMS-D-14-00245.1

Soria JLA, Switzer AD, Pilarczyk JE, Siringan FP, Khan NS, Fritz HM (2017) Typhoon Haiyan overwash sediments from Leyte Gulf coastlines show local spatial variations with hybrid storm and tsunami signatures. *Sedimentary Geology* 358: 121–138. https://doi.org/10.1016/j.sedgeo.2017.06.006

Stone GW, Liu B, Pepper DA, Wang P (2004) The importance of extratropical and tropical cyclones on the short-term evolution of barrier islands along the northern Gulf of Mexico, USA. *Marine Geology* 210: 63–78. https://doi.org/10.1016/j.margeo.2004.05.021

Suerte LO, Yumul GP, Tamayo RA, Dimalanta CB, Zhou M, Maury RC, Polvé M, Balce CL (2005) Geology, geochemistry and U-Pb SHRIMP age of the Tacloban Ophiolite Complex, Leyte Island (Central Philippines): Implications for the existence and extent of the Proto-Philippine Sea Plate. *Resource Geology* 55: 207–216. https://doi.org/10.1111/j.1751-3928.2005.tb00242.x

Switzer AD, Felix RP, Soria JLA, Shaw TA (2020) A comparative study of the 2013 typhoon Haiyan overwash sediments from a coastal cave and beach system at Salcedo, Eastern Samar, central Philippines. *Marine Geology* 419: 106083. https://doi.org/10.1016/j.margeo.2019.106083

Szczuciński W (2020) Post-depositional changes to tsunami deposits and their preservation potential. Engel M, Pilarczyk J, May SM, Brill D, Garrett E (eds) *Geological records of tsunamis and other extreme waves:* 443–469. Amsterdam. https://doi.org/10.1016/B978-0-12-815686-5.00021-3

Tablazon J, Lagmay AMF, Ladiero C, Puno JV, Suarez JK, Santiago J (2016) Storm surge inundation validation in Daram, Samar during Typhoon Hagupit (2014). *Project NOAH Open-File Reports* 5: 20–29.

Tajima Y, Gunasekara KH, Shimozono T, Cruz EC (2016a) Study on locally varying inundation characteristics induced by Super Typhoon Haiyan. Part 1: Dynamic behavior of storm surge and waves around San Pedro Bay. *Coastal Engineering Journal* 58: 1640002. https://doi.org/10.1142/S0578563416400027

Tajima Y, Shimozono T, Gunasekara KH, Cruz EC (2016b) Study on locally varying inundation characteristics induced by Super Typhoon Haiyan. Part 2: Deformation of storm waves on the beach with fringing reef along the east coast of Eastern Samar. *Coastal Engineering Journal* 58: 1640003. https://doi.org/10.1142/S0578563416400039

Takagi H, Esteban M, Shibayama T, Mikami T, Matsumaru R, De Leon M, Thao N, Oyama T, Nakamura R (2017) 2013 Typhoon Haiyan storm surge. *Journal of Flood Risk Management* 10: 42–52. https://doi.org/10.1111/jfr3.12136

Tamura T (2012) Beach ridges and prograded beach deposits as palaeoenvironment records. *Earth-Science Reviews* 114: 279–297. https://doi.org/10.1016/j.earscirev.2012.06.004

Thieler ER, Himmelstoss EA, Zichichi JL, Ergul A (2009) Digital Shoreline Analysis System (DSAS) version 4.0 – an ArcGIS extension for calculating shoreline change. *USGS Open-File Report* 2008-1278. https://doi.org/10.3133/ofr20081278

Traveglia C, Baes AF, Tomas LM (1978) Geology of Samar. Manila.

Wang P, Briggs TMR (2015) Storm-induced morphology changes along barrier islands and poststorm recovery. Shroder JF, Ellis JT, Sherman DJ (eds) *Coastal and marine hazards, risks, and disasters:* 271–306. Amsterdam. http://doi.org/10.1016/B978-0-12-396483-0.00010-8

Wang P, Kirby JH, Haber JD, Horwitz MH, Knorr PO, Krock JR (2006) Morphological and sedimentological impacts of Hurricane Ivan and immediate poststorm beach recovery along the northwestern Florida barrier-island coasts. *Journal of Coastal Research* 22: 1382–1402. https://doi.org/10.2112/05–0440.1

Watanabe M, Bricker J, Goto K, Imamura F (2017) Factors responsible for the limited inland extent of sand deposits on Leyte Island during 2013 Typhoon Haiyan. *Journal of Geophysical Research: Oceans* 122: 2795–2812. https://doi.org/10.1002/2016JC012023

Yoshikawa S, Kanamatsu T, Goto K, Sakamoto I, Yagi M, Fujimaki M, Imura R, Nemoto K, Sakaguchi H (2015) Evidence for erosion and deposition by the 2011 Tohoku-oki tsunami on the nearshore shelf of Sendai Bay, Japan. *Geo-Marine Letters* 35: 315–328. https://doi.org/10.1007/s00367-015-0409-3

Yu F, Switzer AD, Lau AYA, Yeung HYE, Chik SW, Chiu HC, Huang Z, Pile J (2013) A comparison of the post-storm recovery of two sandy beaches on Hong Kong Island, southern China. *Quaternary International* 304: 163–175. https://doi.org/10.1016/j.quaint.2013.04.002

Zalasiewicz J, Williams M, Waters CN, Barnosky AD, Haff P (2014) The technofossil record of humans. *The Anthropocene Review* 1: 34–43. https://doi.org/10.1177/2053019613514953

Authors

Eva Quix
Institute of Geography
University of Cologne
Zülpicher Str. 45
50674 Cologne
Germany
now:
Directorate-General for European Civil Protection and Humanitarian Aid Operations (ECHO)
ECHO.A/4 – Civil Protection
Emergency Response Capabilities
European Commission
1049 Brussels
Belgium

Dr. Max Engel (corresponding author)
https://doi.org/0000-0002-2271-4229
max.engel@uni-heidelberg.de
Institute of Geography
Heidelberg University
Im Neuenheimer Feld 348
69120 Heidelberg
Germany

Dr. Fabian Boesl
https://doi.org/0000-0003-4650-6149
School of Science
Edith Cowan University
Joondalup
Western Australia, 6027
Australia

Lia A. L. Gonzalo
Nationwide Operational Assessment of Hazards (NOAH)
Resilience Institute
University of the Philippines Diliman
Quezon City
The Philippines
Now:
Start Network/CARE Philippines
26 Timog Ave
Diliman
Quezon City
The Philippines

Francesca V. Llanes
https://doi.org/0000-0002-9159-8698
Mark A. C. Bahala
Nationwide Operational Assessment of Hazards (NOAH)
Resilience Institute
University of the Philippines Diliman
Quezon City
The Philippines

Rodrigo C. Eco
https://doi.org/0000-0003-1603-6481
College of Social Work and Community Development
University of the Philippines Diliman
Quezon City
The Philippines

Jan A. M. Galang
Philearth Consultancy Inc.
Diamond St
San Fernando
Pampanga
The Philippines

PD Dr. Dominik Brill
https://doi.org/0000-0001-8637-4641
S. Matthias May
https://doi.org/0000-0001-6762-7500
Prof. Dr. Helmut Brückner
https://doi.org/0000-0002-2130-5394
Institute of Geography
University of Cologne
Zülpicher Str. 45
50674 Cologne
Germany